mathematics

MDPI

Article

Predefined-Time Adaptive Command Filter Control for Nonstrict-Feedback Nonlinear Systems with Input Delay and Unmodeled Dynamics

Mohamed Kharrat [1] and Paolo Mercorelli [2,*]

[1] Mathematics Department, College of Science, Jouf University, Sakaka 71388, Saudi Arabia; mkharrat@ju.edu.sa
[2] Institute for Production Technology and Systems, Leuphana University of Lueneburg, 21335 Lueneburg, Germany
* Correspondence: paolo.mercorelli@leuphana.de

Abstract

This work addresses the tracking control problem of nonstrict-feedback nonlinear systems affected by unmodeled dynamics and input delays, which significantly complicate controller design and degrade system performance. To overcome these challenges, a predefined-time adaptive control framework is developed. A command-filtered backstepping scheme is employed to reduce computational complexity, while an error compensation mechanism is introduced to counteract the inaccuracies caused by command filtering. The unknown nonlinear dynamics are approximated using radial basis function-based estimators, and a dynamic auxiliary signal is designed to mitigate the effects of unmodeled dynamics. Input delays are handled by integrating Padé approximation with an intermediate compensating variable. The proposed control strategy guarantees uniform boundedness of all closed-loop signals and ensures that the tracking error converges to a small neighborhood of the desired trajectory within a predefined time. Simulation results and comparative studies are provided to demonstrate the effectiveness and advantages of the proposed method.

Keywords: nonlinear systems; adaptive control; unmodeled dynamics; input delay; command-filters

MSC: 93C10; 93C40; 37N35

Academic Editors: Libor Pekař, Mengjie Song and Radek Matušů

Received: 1 December 2025
Revised: 14 December 2025
Accepted: 18 December 2025
Published: 20 December 2025

1. Introduction

Over recent decades, adaptive control strategies for nonlinear systems have attracted considerable research attention [1–3]. Among these, adaptive backstepping control stands out for its effectiveness in managing system uncertainties. This method offers a systematic framework for controller design and has been widely applied to nonlinear control problems [4–6]. Despite their strengths, traditional backstepping methods still face two critical challenges. The first is dealing with unknown nonlinear functions that are not linearly parameterized. The second involves the rapid growth in computational complexity due to the recursive structure of the design [7–10]. To approximate unknown nonlinearities, fuzzy logic systems and neural networks have been employed as universal function approximators. Their integration with backstepping techniques has led to the development of numerous adaptive control methods for uncertain nonlinear systems [11–13]. However, the

issue of computational burden remains, as each step requires calculating virtual control signals and their derivatives, significantly increasing complexity.

To mitigate this challenge, the dynamic surface control (DSC) technique was introduced. By incorporating filters to process virtual control signals, DSC eliminates the need for repeated differentiation and thus reduces computational demands. However, filter-induced approximation errors are often overlooked, which can degrade control performance. To address this limitation, command filter-based control strategies have been developed [14,15]. In this approach, virtual control signals are passed through command filters, whose outputs substitute for signal derivatives, while an error compensation mechanism reduces filter-induced inaccuracies and this framework has enabled several advancements in adaptive control [16–18]. For example, adaptive neural control strategy incorporating command filters has been developed for nonstrict-feedback nonlinear systems subject to actuator constraints, achieving both computational efficiency and reliable tracking performance [19]. An alternative research direction involves the development of adaptive control frameworks utilizing command filters to achieve asymptotic tracking in nonlinear systems subject to uncertainties, time-varying dynamics, and external perturbations [20]. To further address randomness and stochastic effects, advanced command filter-based adaptive control strategies with prescribed performance constraints have been introduced, ensuring that the tracking error consistently stays within designer-specified limits despite the presence of modeling uncertainties and disturbances [21].

In practical nonlinear systems, factors such as sensor noise, modeling inaccuracies, and simplifications introduced during system representation often give rise to unmodeled dynamics. It has been demonstrated that such neglected dynamics can significantly impair the effectiveness of the control system and, in certain situations, may even compromise the stability of the closed-loop configuration [22,23]. To address this issue, the use of auxiliary dynamic signals has been recognized as an effective strategy for compensating unmodeled dynamics in real time. In recent years, increasing attention has been directed toward this challenge, and significant progress has been made through the development of advanced control methodologies specifically designed to handle such uncertainties and ensure reliable system operation [24–26]. For instance, adaptive fuzzy asymptotic tracking control has been proposed for nonlinear systems with unmodeled dynamics and quantized actuators, where stable tracking has been achieved despite coarse actuator resolution and unknown system behaviors [27]. An adaptive fault-tolerant control strategy has been used for nonstrict-feedback nonlinear systems that involve unknown dynamics and output dead-zone nonlinearities. To effectively address the challenges arising from structural uncertainties and input nonlinearities, multi-dimensional Taylor networks have been employed due to their strong functional approximation capabilities [28]. In addition, barrier Lyapunov function-based adaptive control has been used to regulate stochastic nonlinear systems subject to full-state constraints, unknown dead-zone characteristics, and unmodeled dynamic behaviors [29].

In many practical applications, time delays are inevitable due to limitations in signal transmission, data processing, or material transport. These delays have been identified as a critical factor in control system design, as they can severely compromise system stability and degrade performance [30,31]. Among the various types of delays, input delays are particularly common and often arise from physical characteristics of the system or communication lags within control loops. Although numerous control strategies have been developed to address input delays in linear systems, real-world systems are frequently nonlinear and subject to uncertainties such as external disturbances, modeling errors, and structural complexities [32,33]. Therefore, developing control methods capable of managing both nonlinear dynamics and input delays has been of significant practical importance.

Over the past few years, the design of adaptive controllers for nonlinear systems with uncertain dynamics and delayed inputs has attracted considerable research attention, resulting in notable progress both theoretically and practically [34,35]. As an example, a neural network-based adaptive control framework has been introduced for nonstrict-feedback nonlinear systems affected by input delays and asymmetric, time-varying state constraints. This approach effectively compensates for input delays while handling varying constraint bounds, all while maintaining system stability [36]. Moreover, fault-tolerant adaptive strategies have been employed to manage systems with uncertain parameters, unknown actuator malfunctions, and input time delays, thereby providing resilience against faults and delay-induced degradation [37]. In another development, adaptive neural control techniques have been extended to stochastic nonstrict-feedback systems with delayed inputs, achieving consistent tracking performance even in the presence of random disturbances and control latency [38].

In real-world applications, the convergence time of control systems is a critical factor, directly influencing operational efficiency and cost-effectiveness. Nevertheless, many traditional control methodologies do not explicitly ensure system convergence within a specified time frame, which is particularly important in safety-critical and time-sensitive scenarios. To address this limitation, time-constrained control techniques such as finite-time and fixed-time control have been developed [39,40]. Finite-time control ensures that system states reach equilibrium in a finite duration, but the convergence period depends on the initial conditions, making it uncertain when such conditions are unknown [41]. Fixed-time control improves upon this by ensuring convergence within a fixed upper bound that remains independent of the initial state [42]. However, fixed-time control also presents notable limitations. First, the actual convergence time observed in practice may deviate considerably from theoretical predictions, undermining reliability. Second, both finite-time and fixed-time schemes lack tunability, as the convergence period cannot be explicitly prescribed and is instead influenced by various control parameters [43–45]. To overcome these drawbacks, the predefined-time control framework has been proposed. This approach allows the designer to explicitly set the desired convergence time, guaranteeing that it is unaffected by the system's initial state and tuning parameters [46,47]. Predefined-time control offers rapid and precise convergence, along with enhanced robustness and timing predictability, making it especially appealing for practical engineering systems [48–52]. Recent advances in this area include predefined-time adaptive fuzzy control technique for nonlinear systems with actuator saturation and delay constraints, which ensure reliable tracking under physical and temporal limitations [53]. Another notable development is the predefined-time fuzzy adaptive decentralized control strategy tailored for interconnected systems facing multiple actuator constraints, facilitating coordinated and robust subsystem control [54]. Furthermore, predefined-time adaptive control with quantized tracking has been introduced for switched nonlinear systems using a command-filtered backstepping framework, effectively handling quantization and switching while ensuring convergence within the assigned time frame [55]. Predefined-time control for full-state constrained nonlinear systems has been studied using an event-triggered approach, incorporating a command-filtering-based error compensation method to achieve fast convergence while maintaining all state constraints [56].

Although numerous control strategies have been proposed to address either unmodeled dynamics or input delays in nonstrict-feedback nonlinear systems, limited attention has been given to scenarios where both challenges occur simultaneously within a predefined-time framework. This gap in the literature forms a key motivation for the present study. In real-world applications, unmodeled dynamics and input delays often coexist, posing significant difficulties for controller design and stability analysis. Inspired by these practical

considerations and existing research, this work develops a predefined-time adaptive control approach for nonlinear systems subject to both unmodeled dynamics and input delay. The key contributions of this study are summarized as follows:

(1) This study presents the proposed predefined-time adaptive control method for nonstrict-feedback nonlinear systems affected by unmodeled dynamics and input delays. Unlike conventional finite-time control [41], where convergence depends on the initial state, and fixed-time control [42], which cannot explicitly prescribe the settling time, the proposed predefined-time method allows the convergence time to be directly specified in advance. This ensures predictable and precise settling independent of initial conditions and provides enhanced reliability and suitability for real-time and safety-critical applications. Furthermore, the proposed predefined-time method simultaneously addresses system nonlinearities, unmodeled dynamics, and input delays within a unified adaptive framework, offering improved performance and consistency compared to existing approaches.

(2) To simultaneously manage the challenges posed by unmodeled dynamics and input delay, a dynamic compensator is introduced to estimate the unknown dynamics, while a Padé approximation is employed alongside an intermediate signal to mitigate the impact of the delayed input. The control framework integrates adaptive backstepping with the command filtering approach, effectively reducing the computational burden typically seen in conventional backstepping methods by avoiding derivative explosion. To further enhance performance, tailored compensation terms are designed to counteract the filtering errors introduced during the command generation process, resulting in better trajectory tracking. The proposed predefined-time control scheme guarantees that all signals within the closed-loop system remain bounded and that the tracking error converges to a small vicinity of the reference trajectory within a prescribed time, regardless of the system's initial state.

The structure of the paper is as follows. Section 2 presents the problem formulation along with relevant preliminary concepts. Section 3 details the development of the proposed adaptive control strategy and provides a comprehensive stability analysis. In Section 4, simulation results are offered to demonstrate the effectiveness and robustness of the designed control scheme. Finally, Section 5 concludes the paper by summarizing the main findings and contributions.

Notation 1. *The symbol $\|x\|$ denotes the Euclidean norm of a vector x. The operator $a \circ b$ represents the Hadamard (element-wise) product of vectors a and b. The vector $x = [x_1, x_2, \ldots, x_n]^T$ denotes an n-dimensional state. The symbol $\mathbb{R}$ denotes the set of real numbers, while $\mathbb{R}_+ = \{x \in \mathbb{R} \mid x > 0\}$ and $\mathbb{R}_{\geq 0} = \{x \in \mathbb{R} \mid x \geq 0\}$ represent the sets of positive and nonnegative real numbers, respectively. The set $\mathbb{R} \setminus \{0\}$ consists of all real numbers except zero, and $\mathbb{R}^n$ denotes the n-dimensional Euclidean space.*

2. Problem Formulation and Preliminaries

Consider the following class of nonstrict-feedback nonlinear systems as

$$\begin{cases} \dot{\xi} = q(t, \xi, x), \\ \dot{x}_i = g_i(x)x_{i+1} + f_i(x) + \Delta_i(t, \xi, x), \quad i = 1, \ldots, n-1, \\ \dot{x}_n = g_n(x)u(t-\tau) + f_n(x) + \Delta_n(t, \xi, x), \\ y = x_1, \end{cases} \tag{1}$$

where $x = [x_1, x_2, \ldots, x_n]^T \in \mathbb{R}^n$ denotes the state vector, $u \in \mathbb{R}$ is the control input, $y \in \mathbb{R}$ is the system output, and τ denotes the unknown input delay, which is assumed to

be a positive constant. The functions $f_i(x)$ are unknown but assumed to be smooth and nonlinear, and $\xi \in \mathbb{R}^{n_i}$ represents the unmodeled dynamics. Each function $g_i(x)$ is a known, continuously differentiable function that satisfies the boundedness condition $0 < g_i(x) \leq \bar{g}_i$, where $\bar{g}_i$ denotes a known positive upper bound. The expressions $\Delta_i(t, \xi, x)$ for $i = 1, \ldots, n$ represent unknown disturbances arising due to unmodeled dynamics. Assume that the desired trajectory is given by the vector $x_d = [y_d, \dot{y}_d]^T$, which belongs to the compact set $\Omega_d = \{x_d \mid y_d^2 + \dot{y}_d^2 \leq B\}$, where B is a specified positive constant. The trajectory $x_d(t)$ is considered to be smooth, and its components are available for measurement.

The goal is to design an adaptive control input $u(t)$ that ensures the system output $y(t)$ accurately tracks the desired reference signal $y_d(t)$ over time. Moreover, it is required that all signals within the closed-loop system remain uniformly bounded, and the tracking error converges to zero within a user-specified, fixed time interval through appropriate tuning of the controller parameters.

Consider the following general nonlinear system as

$$\dot{z} = f(z, \rho), \tag{2}$$

where $z \in \mathbb{R}^n$ represents the system state, $f : \mathbb{R}^n \to \mathbb{R}^n$ is a nonlinear function, and $\rho \in \mathbb{R}^\ell$ denotes a vector of design parameters. It is assumed that the origin is an equilibrium point of system (2), and the initial condition is given by $z(0) = z_0$.

Remark 1. *The condition that $g_n(x)$ remains positive and bounded in (1) serves as a controllability requirement for the last subsystem. Since the control input $u(t - \tau)$ enters the dynamics only through $g_n(x)$, maintaining $g_n(x) > 0$ guarantees that the control channel is effective and prevents loss of influence of the input on the system. This ensures that the overall nonstrict-feedback system remains controllable through the recursive design steps. Such a condition is standard in adaptive backstepping frameworks and is satisfied by many physical systems in which the input gain does not vanish during operation.*

Definition 1 ([50]). *The system described by (2) is considered to be fixed-time-stable if it exhibits global asymptotic stability and there exists a constant $T_{\max} > 0$ such that the settling time $T(z_0)$ satisfies the inequality $T(z_0) \leq T_{\max}$ for all initial states $z_0 \in \mathbb{R}^n$. Here, $T_{\max}$ represents a uniform upper limit that does not depend on the initial condition.*

Definition 2 ([50]). *The system in (2) is defined as predefined-time-stable if it meets the criteria for fixed-time stability, and furthermore, the settling time adheres to the bound $T(z_0) \leq T_c$ for every $z_0 \in \mathbb{R}^n$, where $T_c \in \mathbb{R}_+$ is a user-specified constant.*

Definition 3 ([49]). *Let $T_c, q \in \mathbb{R}_+$ be given constants. The system described in (2) is said to possess predefined-time ultimate boundedness if there exists a tunable parameter vector $\rho \in \mathbb{R}^\ell$ such that, for any initial state $z_0 \in \mathbb{R}^n$, the state trajectory satisfies $\|z(t)\| \leq q$ for all $t \geq T_c$.*

Lemma 1 ([49]). *Consider system (2). Assume that there exists a Lyapunov candidate function $V(z)$ such that for all states satisfying $\|z\| \geq \mu$, the following condition is met:*

$$\dot{V}(z) \leq -\frac{\alpha_0}{p} \exp(-\beta V^p(z)) V^{1-p}(z), \tag{3}$$

where the constants $\alpha_0, \beta, \mu \in \mathbb{R}_+$, and the parameter p satisfies $0 \leq p < 1$. If $V(z)$ is a continuous, non-negative, and radially unbounded function, then the system (2) is considered to exhibit predefined-time ultimate boundedness. Furthermore, the settling time required for the system state to enter the bounded region is guaranteed to satisfy $T_c \leq \frac{1}{\alpha_0 \beta}$.

Lemma 2 ([51]). *The unmodeled dynamics described by $\dot{\xi} = q(t, \xi, x)$ is considered to be exponentially input-to-state practically stable (exp-IspS) if there exists a Lyapunov function $V(\xi)$ satisfying the following conditions:*

$$\bar{\alpha}_1(\|\xi\|) \leq V(\xi) \leq \bar{\alpha}_2(\|\xi\|), \tag{4}$$

$$\frac{\partial V(\xi)}{\partial \xi} q(t, \xi, x) \leq -cV(\xi) + \gamma(|x_1|) + d, \tag{5}$$

where $\bar{\alpha}_1(\cdot)$ and $\bar{\alpha}_2(\cdot)$ are class $\mathcal{K}_\infty$ functions, $\gamma(\cdot)$ is a known function also belonging to class $\mathcal{K}_\infty$, and c, d are positive constants.

Lemma 3 ([51]). *Let us consider the system $\dot{\xi} = q(t, \xi, x)$, and assume that $V(\xi)$ is an exponential input-to-state practically stable (exp-IspS) Lyapunov function. Under this condition, there exists a finite time $T_0 \geq 0$ defined as $T_0 = \max\left\{0, \frac{\ln[V(\xi_0)/v_0]}{c-\bar{c}}\right\}$, along with a nonnegative function $D(t_0, t)$ for all $t \geq t_0$, and an auxiliary dynamic signal $v(t)$ such that the inequality $V(\xi(t)) \leq v(t) + D(t_0, t)$ holds. The signal $v(t)$ evolves according to the differential equation:*

$$\dot{v} = -\bar{c}v + \bar{\gamma}(|x_1|) + d, \quad v(t_0) = v_0 > 0, \tag{6}$$

with $\bar{c} \in (0, c)$, t_0 as the initial time, and $\xi_0 = \xi(t_0)$. The function $\bar{\gamma}(|x_1|)$ is of class $\mathcal{K}_\infty$ and satisfies $\bar{\gamma}(|x_1|) \geq \gamma(|x_1|)$, and $D(t_0, t) = \max\left\{0, e^{-c(t-t_0)}V(\xi_0) - e^{-\bar{c}(t-t_0)}v_0\right\}$.

Lemma 4 ([50]). *Let $x = (x_1, x_2, \ldots, x_n)$ and $y = (y_1, y_2, \ldots, y_n)$ be two sequences of real numbers that are similarly ordered, i.e., either $x_1 \leq x_2 \leq \cdots \leq x_n$ and $y_1 \leq y_2 \leq \cdots \leq y_n$, or $x_1 \geq x_2 \geq \cdots \geq x_n$ and $y_1 \geq y_2 \geq \cdots \geq y_n$. Then, the following inequality holds:*

$$\sum_{i=1}^{n} x_i y_i \geq \frac{1}{n}\left(\sum_{i=1}^{n} x_i\right)\left(\sum_{i=1}^{n} y_i\right). \tag{7}$$

According to the universal approximation theorem for radial basis function neural networks (RBFNNs) [14], for any continuous function $h_i(Z_i)$ defined on a compact set $Z_i \subset \Omega_{Z_i}$ and for any desired approximation accuracy $\varepsilon > 0$, there exists a sufficiently large number of nodes N_i such that

$$h_i(Z_i) = W_i^{*T}\Phi_i(Z_i) + \delta_i(Z_i), \tag{8}$$

where $\delta_i(Z_i)$ denotes the approximation error and satisfies $|\delta_i(Z_i)| \leq \varepsilon$. The optimal weight vector W_i^* is defined by

$$W_i^* := \arg \min_{W_i \in \mathbb{R}^{N_i}} \left[\sup_{Z_i \in \Omega_{Z_i}} \left\|W_i^T \Phi_i(Z_i) - f_i(Z_i)\right\|\right]. \tag{9}$$

The basis function vector is given by $\Phi_i(Z_i) = [\Phi_{i1}(Z_i), \ldots, \Phi_{iN_i}(Z_i)]^\top, \quad i = 1, \cdots, n$, where each basis function typically takes the Gaussian form

$$\Phi_{ij}(Z_i) = \exp\left(-\frac{(Z_i - \mu_{ij})^\top (Z_i - \mu_{ij})}{\eta_{ij}^2}\right), \quad j = 1, 2, \cdots, N_i, \tag{10}$$

with $\mu_{ij} = [\mu_{ij1}, \cdots, \mu_{ijl}]^\top$ representing the center vector and $\eta_{ij} > 0$ the width (or spread) parameter of the jth radial basis function.

Lemma 5 ([14]). *Let $Z = [Z_1, \ldots, Z_n]$, $X = [Z_{i_1}, \ldots, Z_{i_m}]$, where $\{i_1, \ldots, i_m\}$ is a subsequence of $\{1, \ldots, n\}$. Let $\mu = [\mu_1, \ldots, \mu_n]$ and $\sigma = [\sigma_1, \ldots, \sigma_n]$ be two constant vectors with $\sigma_i > 0$ for all i. Define the functions $\Phi(Z)$ and $\Phi(X)$ as*

$$\Phi(Z) = \prod_{j=1}^{n} \exp\left(-\frac{(Z_j - \mu_j)^2}{2\sigma_j^2}\right), \tag{11}$$

$$\Phi(X) = \prod_{j=1}^{m} \exp\left(-\frac{(Z_{i_j} - \mu_{i_j})^2}{2\sigma_{i_j}^2}\right). \tag{12}$$

Then, it holds that $\Phi(Z) \leq \Phi(X)$.

3. Controller Design and Stability Analysis

In this section, a robust adaptive control strategy is proposed for a class of nonlinear systems characterized by a nonstrict-feedback structure, where the presence of unmodeled dynamics and delayed control inputs poses significant challenges. To effectively manage the input delay, the design integrates a sequence of coordinate transformations along with an approximation technique based on Padé rational functions. The step-by-step controller synthesis is elaborated as follows.

To cope with the complications introduced by delayed inputs, the strategy draws inspiration from the framework described in [34], employing the Padé approximation to represent the delay element. Utilizing the delay property from Laplace transform theory, the following expression is obtained:

$$\mathcal{L}\{u(t-\tau)\} = e^{-\tau s}\mathcal{L}\{u(t)\} = \frac{e^{-\tau s/2}}{e^{\tau s/2}}\mathcal{L}\{u(t)\}, \tag{13}$$

where s denotes the Laplace variable and $\mathcal{L}\{u(t)\}$ is the Laplace transform of $u(t)$. Using the Pade approximation, the exponential delay term can be approximated as

$$e^{-\tau s}\mathcal{L}\{u(t)\} \approx \frac{1 - \frac{\tau s}{2}}{1 + \frac{\tau s}{2}}\mathcal{L}\{u(t)\}. \tag{14}$$

Let $x_{n+1}(t)$ be an intermediate variable defined such that

$$\frac{1 - \frac{\tau s}{2}}{1 + \frac{\tau s}{2}}\mathcal{L}\{u(t)\} = \mathcal{L}\{x_{n+1}(t)\} - \mathcal{L}\{u(t)\}. \tag{15}$$

Rearranging (15) yields

$$2\mathcal{L}\{u(t)\} = \mathcal{L}\{x_{n+1}(t)\} + \frac{\tau s}{2}\mathcal{L}\{x_{n+1}(t)\}. \tag{16}$$

Taking the inverse Laplace transform, one has

$$\dot{x}_{n+1} = \frac{4}{\tau}u - \frac{2}{\tau}x_{n+1}. \tag{17}$$

Introducing the variable $\lambda = \frac{2}{\tau}$, one has

$$\dot{x}_{n+1} = 2\lambda u - \lambda x_{n+1}. \tag{18}$$

Based on the above transformations, system (1) can be further rewritten as

$$\begin{cases} \dot{\xi} = q(t,\xi,x), \\ \dot{x}_i = g_i(x)x_{i+1} + f_i(x) + \Delta_i(t,\xi,x), \quad i = 1,\ldots,n-1, \\ \dot{x}_n = x_{n+1} - g_n(x)u + f_n(x) + \Delta_n(t,\xi,x), \\ \dot{x}_{n+1} = -\lambda x_{n+1} + 2\lambda g_n(x)u, \\ y = x_1, \end{cases} \tag{19}$$

To design an adaptive controller, we begin by applying the following coordinate transformation

$$\begin{cases} z_1 = x_1 - y_d, \\ z_i = x_i - \omega_i, \quad i = 2,\ldots,n-1, \\ z_n = x_n - \omega_n + x_{n+1}/\lambda, \end{cases} \tag{20}$$

where ω_i denotes the response of a first-order dynamic filter associated with the virtual control signal α_{i-1}, and is characterized by the following relation

$$\tau_i\dot{\omega}_i = \alpha_{i-1} - \omega_i, \quad \omega_i(0) = \alpha_{i-1}(0), \quad i = 2,\ldots,n, \tag{21}$$

with $\tau_i > 0$ being the filter time constant.

For convenience, define the following shorthand notations $\bar{x}_i = [x_1,\ldots,x_i]^T$, $\bar{s}_i = [s_1,\ldots,s_i]^T$, $\bar{\hat{\theta}}_i = [\hat{\theta}_1,\ldots,\hat{\theta}_i]^T$, $\bar{\eta}_i = [\eta_1,\ldots,\eta_i]^T$.

Remark 2. *Command filters are introduced in the backstepping design to avoid repeated differentiation of virtual control signals and to simplify the overall computational process. However, the filtering operation causes a mismatch between the ideal virtual control signal and the filtered output. This mismatch, if unaddressed, may accumulate during the recursive design procedure and degrade the tracking performance. To overcome this effect, a compensating signal is included in each design step. This signal dynamically estimates the filtering error and injects a correction term back into the control law. As a result, the combined effect of the filtered signal and the compensation term closely reproduces the ideal virtual control, thereby preserving the accuracy of the backstepping procedure and ensuring the robustness and predefined-time convergence of the closed-loop system.*

Remark 3. *It is important to note that the variable x_{n+1} is not an actual state of system (1); rather, it is an auxiliary variable introduced in the design of the n-th subsystem to approximate the delayed input effect. Due to the unknown time delay τ, the parameter λ becomes uncertain, which in turn introduces uncertainty into the behavior of x_{n+1}. Referring to (19) and (20), as well as the transformed variable $z_n = x_n - \omega_n + x_{n+1}/\lambda$, the actual control input u is designed in such a way that it compensates for the intermediate variable x_{n+1} and effectively counteracts the adverse effects introduced by the input delay.*

Next, define the compensated tracking errors as

$$s_i = z_i - \eta_i, \quad i = 1,\ldots,n, \tag{22}$$

where η_i represents the compensating signal constructed according to the following formulation as

$$\begin{cases} \dot{\eta}_i = -\dfrac{\eta_i}{2p_{i3}T_{ci3}}\exp\left(\left(\frac{1}{2}\eta_i^2\right)^{p_{i3}}\right)\left(\frac{1}{2}\eta_i^2\right)^{-p_{i3}} + g_i(\omega_{i+1} - \alpha_i) + g_i\eta_{i+1}, \quad i = 1,\ldots,n-1, \\ \dot{\eta}_n = -\dfrac{\eta_n}{2p_{n3}T_{cn3}}\exp\left(\left(\frac{1}{2}\eta_n^2\right)^{p_{n3}}\right)\left(\frac{1}{2}\eta_n^2\right)^{-p_{n3}}. \end{cases} \tag{23}$$

with $p_{ik} \in (0, \frac{1}{2})$ and $T_{cik} > 0$ for $i = 1, \ldots, n$ and $k = 1, 2, 3$ are user-defined design parameters. Notably, the expression $\exp\left(\left(\frac{1}{2}\eta_i^2\right)^{p_{i3}}\right)\left(\frac{1}{2}\eta_i^2\right)^{-p_{i3}}\eta_i$ simplifies to $\exp\left(\left(\frac{1}{2}\eta_i^2\right)^{p_{i3}}\right)\left(\frac{1}{2}\right)^{-p_{i3}}\eta_i^{1-2p_{i3}}$, which remains well-defined at $\eta_i = 0$, due to the condition $0 < p_{i3} < \frac{1}{2}$ ensuring that the exponent $1 - 2p_{i3}$ is positive. This effectively eliminates any potential singularity in the formulation.

Step 1: By utilizing (1), (20), (22), and (23), the time derivative of the compensated tracking error s_1 can be expressed as

$$\dot{s}_1 = \frac{\eta_1}{2p_{13}T_{c13}}\exp\left(\left(\tfrac{1}{2}\eta_1^2\right)^{p_{13}}\right)\left(\tfrac{1}{2}\eta_1^2\right)^{-p_{13}} + g_1 s_2 + g_1\alpha_1 + f_1 + \Delta_1(t,\xi,x) - \dot{y}_d. \tag{24}$$

Define the following Lyapunov function as

$$V_1 = \frac{1}{2}s_1^2 + \frac{1}{2}\tilde{\theta}_1^2, \tag{25}$$

where $\tilde{\theta}_1 = \theta_1 - \hat{\theta}_1$ denotes the parameter estimation error.

Taking the time derivative of V_1 and using (24), we obtain

$$\dot{V}_1 = s_1\left[\frac{\eta_1}{2p_{13}T_{c13}}\exp\left(\left(\tfrac{1}{2}\eta_1^2\right)^{p_{13}}\right)\left(\tfrac{1}{2}\eta_1^2\right)^{-p_{13}} + g_1 s_2 + g_1\alpha_1 + f_1 + \Delta_1(t,\xi,x) - \dot{y}_d\right] - \tilde{\theta}_1\dot{\hat{\theta}}_1. \tag{26}$$

Assume that the unknown disturbance term $\Delta_i(t,\xi,x)$ is bounded as follows:

$$|\Delta_i(t,\xi,x)| \le \psi_{i1}(\|\bar{x}_i\|) + \psi_{i2}(\|\xi\|),$$

where $\psi_{i1}(\cdot)$ is a continuous, nonnegative, and unspecified function, and $\psi_{i2}(\cdot)$ is also unknown, continuous, and monotonically nondecreasing. Based on Equation (4), the norm of the disturbance state ξ can be estimated by $\|\xi\| \le \bar{\alpha}_1^{-1}(V(\xi))$. Furthermore, utilizing the result from Lemma 3, one can find a positive constant D_0 such that for all $t \ge 0$, the following inequality holds, $\|\xi\| \le \bar{\alpha}_1^{-1}(v + D_0)$, where $v(t)$ denotes the dynamic signal defined in Lemma 3. This inequality serves as a key tool in handling the effect of unknown disturbances during the design of the adaptive control law.

Applying Young's inequality, we can estimate the cross-term involving the disturbance as

$$\begin{aligned} s_1\Delta_1(t,\xi,x) &\le |s_1||\Delta_1(t,\xi,x)| \\ &\le |s_1|\psi_{11}(\|x_1\|) + |s_1|\psi_{12}(\|\xi\|) \\ &\le s_1^2\psi_{11}^2(\|x_1\|) + s_1^2\psi_{12}^2(\bar{\alpha}_1^{-1}(v + D_0)) + \frac{1}{2}. \end{aligned} \tag{27}$$

Let

$$h_1(Z_1) = f_1 + s_1\psi_{11}^2(\|x_1\|) + s_1\psi_{12}^2 \circ \bar{\alpha}_1^{-1}(v + D_0), \tag{28}$$

where $Z_1 = [x^\top, s_1, v]^T$. By using RBFNNs, the unknown nonlinear function $h_1(Z_1)$ can be approximated using a radial basis function neural network as

$$h_1(Z_1) = W_1^{*\top}\Phi_1(Z_1) + \delta_1(Z_1), \tag{29}$$

where W_1^* is the ideal weight vector, $\Phi_1(Z_1)$ is the known basis function vector, and $\delta_1(Z_1)$ is the bounded approximation error.

Using Young's inequality and Lemma 5, the following bounds hold

$$s_1 h_1(Z_1) \le \frac{1}{2a_1^2} s_1^2 \theta_1 \Phi_1^\top(X_1)\Phi_1(X_1) + \frac{a_1^2}{2}, \tag{30}$$

$$s_1 \delta_1(Z_1) \le \frac{1}{2} s_1^2 + \frac{1}{2}\epsilon_1^2, \tag{31}$$

where $\theta_1 = \|W_1^*\|^2$, $X_1 = [x_1, s_1, v]^T$, and ϵ_1 is a continuous function that satisfies $|\delta_1(Z_1)| \le \epsilon_1(\bar{s}_n^T, \bar{\hat{\theta}}_n^T, y_d, \dot{y}_d)$.

The virtual control input α_1 and the adaptive law for the parameter estimate $\hat{\theta}_1$ are designed as

$$\begin{aligned}\alpha_1 = \frac{1}{g_1}\Bigg[&- \frac{s_1}{2p_{11}T_{c11}} \exp\left(\left(\tfrac{1}{2}s_1^2\right)^{p_{11}}\right)\left(\tfrac{1}{2}s_1^2\right)^{-p_{11}} \\ &- \frac{\eta_1}{2p_{13}T_{c13}} \exp\left(\left(\tfrac{1}{2}\eta_1^2\right)^{p_{13}}\right)\left(\tfrac{1}{2}\eta_1^2\right)^{-p_{13}} \\ &- \frac{1}{2a_1^2} s_1 \hat{\theta}_1 \Phi_1^T \Phi_1 - \frac{1}{2}s_1 + \dot{y}_d \Bigg],\end{aligned} \tag{32}$$

$$\dot{\hat{\theta}}_1 = -\frac{r_1}{p_{12}T_{c12}} \exp\left(\left(\tfrac{1}{2}\hat{\theta}_1^2\right)^{p_{12}}\right)\left(\tfrac{1}{2}\hat{\theta}_1^2\right)^{\frac{1}{2}-p_{12}}\hat{\theta}_1 + \frac{1}{2a_1^2} s_1^2 \Phi_1^T(X_1)\Phi_1(X_1), \tag{33}$$

where $a_1 > 0, r_1 > 0$ are design constants.

It is important to note that the expression in (32),

$$\exp\left(\left(\tfrac{1}{2}s_1^2\right)^{p_{11}}\right)\left(\tfrac{1}{2}s_1^2\right)^{-p_{11}} s_1 = \exp\left(\left(\tfrac{1}{2}s_1^2\right)^{p_{11}}\right)\left(\tfrac{1}{2}\right)^{-p_{11}} (s_1^2)^{\frac{1}{2}-p_{11}},$$

remains well-defined at $s_1 = 0$ under the condition $0 < p_{11} < \frac{1}{2}$, thereby avoiding singularities in the controller. This argument similarly holds for all $i = 2, \ldots, n$.

By inserting (30)–(33) into (26), one has

$$\begin{aligned}\dot{V}_1 \le &- \frac{1}{p_{11}T_{c11}} \exp\left(\left(\tfrac{1}{2}s_1^2\right)^{p_{11}}\right)\left(\tfrac{1}{2}s_1^2\right)^{1-p_{11}} + \frac{r_1\hat{\theta}_1\tilde{\theta}_1}{p_{12}T_{c12}} \exp\left(\left(\tfrac{1}{2}\hat{\theta}_1^2\right)^{p_{12}}\right)\left(\tfrac{1}{2}\hat{\theta}_1^2\right)^{\frac{1}{2}-p_{12}} \\ &+ \frac{a_1^2}{2} + \frac{\epsilon_1^2}{2} + \frac{1}{2} + g_1 s_1 s_2.\end{aligned} \tag{34}$$

Step i **(**$2 \le i \le n-1$**):** By using (1), (20), (22), and (23), the derivative of the compensated tracking error s_i is given by

$$\dot{s}_i = \frac{\eta_i}{2p_{i3}T_{ci3}} \exp\left(\left(\tfrac{1}{2}\eta_i^2\right)^{p_{i3}}\right)\left(\tfrac{1}{2}\eta_i^2\right)^{-p_{i3}} + g_i s_{i+1} + g_i \alpha_i + f_i + \Delta_i(t, \xi, x) - \dot{\omega}_i. \tag{35}$$

Define the composite Lyapunov function as

$$V_i = V_{i-1} + \frac{1}{2}s_i^2 + \frac{1}{2}\tilde{\theta}_i^2. \tag{36}$$

Taking the time derivative of (36) and using (35), we get

$$\begin{aligned}\dot{V}_i &= \dot{V}_{i-1} + s_i\left[\frac{\eta_i}{2p_{i3}T_{ci3}}\exp\left(\left(\tfrac{1}{2}\eta_i^2\right)^{p_{i3}}\right)\left(\tfrac{1}{2}\eta_i^2\right)^{-p_{i3}} + g_i s_{i+1} + g_i\alpha_i + f_i + \Delta_i(t,\xi,x)\right.\\ &\quad\left. - \dot{\omega}_i\right] - \tilde{\theta}_i\dot{\hat{\theta}}_i\\ &\le -\sum_{j=1}^{i-1}\frac{1}{p_{j1}T_{cj1}}\exp\left(\left(\tfrac{1}{2}s_j^2\right)^{p_{j1}}\right)\left(\tfrac{1}{2}s_j^2\right)^{1-p_{j1}} + \sum_{j=1}^{i-1}\frac{r_j\hat{\theta}_j\tilde{\theta}_j}{p_{j2}T_{cj2}}\exp\left(\left(\tfrac{1}{2}\hat{\theta}_j^2\right)^{p_{j2}}\right)\left(\tfrac{1}{2}\hat{\theta}_j^2\right)^{\frac{1}{2}-p_{j2}}\\ &\quad + \sum_{j=1}^{i-1}\left(\frac{a_j^2}{2}+\frac{\epsilon_j^2}{2}\right) + \frac{i-1}{2} + s_i\left[\frac{\eta_i}{2p_{i3}T_{ci3}}\exp\left(\left(\tfrac{1}{2}\eta_i^2\right)^{p_{i3}}\right)\left(\tfrac{1}{2}\eta_i^2\right)^{-p_{i3}} + g_i s_{i+1} + g_i\alpha_i + f_i\right.\\ &\quad\left. + \Delta_i(t,\xi,x) - \dot{\omega}_i\right] - \tilde{\theta}_i\dot{\hat{\theta}}_i + s_{i-1}s_i.\end{aligned} \tag{37}$$

Analogous to inequality (27), for the i-th step with $2 \le i \le n-1$, we have

$$\begin{aligned}s_i\Delta_i(t,\xi,x) &\le |s_i||\Delta_i(t,\xi,x)| \le |s_i|\psi_{i1}(\|\bar{x}_i\|) + |s_i|\psi_{i2}(\|\xi\|)\\ &\le s_i^2\psi_{i1}^2(\|\bar{x}_i\|) + s_i^2\psi_{i2}^2 \circ \bar{\alpha}_1^{-1}(v + D_0) + \frac{1}{2}.\end{aligned} \tag{38}$$

Define the unknown function

$$h_i(Z_i) = f_i + s_i\psi_{i1}^2(\|\bar{x}_i\|) + s_i\psi_{i2}^2 \circ \bar{\alpha}_1^{-1}(v + D_0), \tag{39}$$

where $Z_i = [x^\top, s_i, v]^\top$ is the regressor vector.

By using RBFNN, $h_i(Z_i)$ can be approximated as

$$h_i(Z_i) = W_i^{*\top}\Phi_i(Z_i) + \delta_i(Z_i). \tag{40}$$

Using Lemma 5 and Young's inequality, one has

$$s_i h_i(Z_i) \le \frac{1}{2a_i^2}s_i^2\theta_i\Phi_i^\top(X_i)\Phi_i(X_i) + \frac{a_i^2}{2}, \tag{41}$$

$$s_i\delta_i(Z_i) \le \frac{1}{2}s_i^2 + \frac{1}{2}\epsilon_i^2, \tag{42}$$

where $\theta_i = \|W_i^*\|^2$, $X_i = [\bar{x}_i^T, s_i, v]^T$, and ϵ_i is a continuous function satisfying $|\delta_i(Z_i)| \le \epsilon_i(\bar{s}_n^T, \bar{\hat{\theta}}_n^T, y_d, \dot{y}_d)$.

The virtual control law α_i and adaptive update law for $\hat{\theta}_i$ are designed as follows:

$$\begin{aligned}\alpha_i = \frac{1}{g_i}\Bigg[&-\frac{s_i}{2p_{i1}T_{ci1}}\exp\left(\left(\tfrac{1}{2}s_i^2\right)^{p_{i1}}\right)\left(\tfrac{1}{2}s_i^2\right)^{-p_{i1}}\\ &-\frac{\eta_i}{2p_{i3}T_{ci3}}\exp\left(\left(\tfrac{1}{2}\eta_i^2\right)^{p_{i3}}\right)\left(\tfrac{1}{2}\eta_i^2\right)^{-p_{i3}}\\ &-\frac{1}{2a_i^2}s_i\hat{\theta}_i\Phi_i^T(X_i)\Phi_i(X_i) - \frac{1}{2}s_i - g_{i-1}s_{i-1} + \dot{\omega}_i\Bigg],\end{aligned} \tag{43}$$

$$\dot{\hat{\theta}}_i = -\frac{r_i}{p_{i2}T_{ci2}}\exp\left(\left(\tfrac{1}{2}\hat{\theta}_i^2\right)^{p_{i2}}\right)\left(\tfrac{1}{2}\hat{\theta}_i^2\right)^{\frac{1}{2}-p_{i2}}\hat{\theta}_i + \frac{1}{2a_i^2}s_i^2\Phi_i^T(X_i)\Phi_i(X_i), \tag{44}$$

where $a_i > 0, r_i > 0$ are design constants.

By inserting (41)–(44) into (37), one has

$$\begin{aligned}\dot{V}_i \leq & -\sum_{j=1}^{i}\frac{1}{p_{j1}T_{cj1}}\exp\left(\left(\tfrac{1}{2}s_j^2\right)^{p_{j1}}\right)\left(\tfrac{1}{2}s_j^2\right)^{1-p_{j1}} \\ & +\sum_{j=1}^{i}\frac{r_j\hat{\theta}_j\tilde{\theta}_j}{p_{j2}T_{cj2}}\exp\left(\left(\tfrac{1}{2}\hat{\theta}_j^2\right)^{p_{j2}}\right)\left(\tfrac{1}{2}\hat{\theta}_j^2\right)^{\frac{1}{2}-p_{j2}} \\ & +\sum_{j=1}^{i}\left(\frac{a_j^2}{2}+\frac{\epsilon_j^2}{2}\right)+\frac{i}{2}+g_is_is_{i+1}.\end{aligned} \tag{45}$$

Step n**:** By differentiating s_n with respect to time and using the expressions from (19), (20), (22), and (23), we obtain

$$\begin{aligned}\dot{s}_n &= \dot{z}_n-\dot{\eta}_n \\ &= \dot{x}_n-\dot{\omega}_n+\frac{x_{n+1}}{\lambda}-\dot{\eta}_n \\ &= x_{n+1}-g_nu+f_n+\Delta_n(t,\xi,x)-\dot{\omega}_n+\frac{1}{\lambda}(-\lambda x_{n+1}+2\lambda g_nu)-\dot{\eta}_n \\ &= g_nu+f_n+\Delta_n(t,\xi,x)-\dot{\omega}_n-\dot{\eta}_n \\ &= \frac{\eta_n}{2p_{n3}T_{cn3}}\exp\left(\left(\tfrac{1}{2}\eta_n^2\right)^{p_{n3}}\right)\left(\tfrac{1}{2}\eta_n^2\right)^{-p_{n3}}+x_{n+1}g_nu+f_n+\Delta_n(t,\xi,x)-\dot{\omega}_n\end{aligned} \tag{46}$$

Define the Lyapunov function as

$$V_n=V_{n-1}+\frac{1}{2}s_n^2+\frac{1}{2}\tilde{\theta}_n^2. \tag{47}$$

Taking the derivative of (47) and using (46), one has

$$\begin{aligned}\dot{V}_n &= \dot{V}_{n-1}+s_n\left[\frac{\eta_n}{2p_{n3}T_{cn3}}\exp\left(\left(\tfrac{1}{2}\eta_n^2\right)^{p_{n3}}\right)\left(\tfrac{1}{2}\eta_n^2\right)^{-p_{n3}}+g_nu+f_n+\Delta_n(t,\xi,x)\right. \\ &\quad \left.-\dot{\omega}_n\right]-\tilde{\theta}_n\dot{\hat{\theta}}_n \\ &\leq -\sum_{j=1}^{n-1}\frac{1}{p_{j1}T_{cj1}}\exp\left(\left(\tfrac{1}{2}s_j^2\right)^{p_{j1}}\right)\left(\tfrac{1}{2}s_j^2\right)^{1-p_{j1}}+\sum_{j=1}^{n-1}\frac{r_j\hat{\theta}_j\tilde{\theta}_j}{p_{j2}T_{cj2}}\exp\left(\left(\tfrac{1}{2}\hat{\theta}_j^2\right)^{p_{j2}}\right)\left(\tfrac{1}{2}\hat{\theta}_j^2\right)^{\frac{1}{2}-p_{j2}} \\ &\quad +\sum_{j=1}^{n-1}\left(\frac{a_j^2}{2}+\frac{\epsilon_j^2}{2}\right)+\frac{n-1}{2}+s_n\left[\frac{\eta_n}{2p_{n3}T_{cn3}}\exp\left(\left(\tfrac{1}{2}\eta_n^2\right)^{p_{n3}}\right)\left(\tfrac{1}{2}\eta_n^2\right)^{-p_{n3}}\right. \\ &\quad \left.+g_nu+f_n+\Delta_n(t,\xi,x)-\dot{\omega}_n\right]-\tilde{\theta}_n\dot{\hat{\theta}}_n+g_{n-1}s_{n-1}s_n.\end{aligned} \tag{48}$$

Similar to (27) and (38), one has

$$\begin{aligned}s_n\Delta_n(t,\xi,x)\leq|s_n|\,|\Delta_n(t,\xi,x)|\leq|s_n|\psi_{n1}(\|x\|)+|s_n|\psi_{n2}(\|\xi\|)\leq s_n^2\psi_{n1}^2(\|x\|) \\ +s_n^2\psi_{n2}^2\circ\bar{\alpha}_1^{-1}(v+D_0)+\frac{1}{2}.\end{aligned} \tag{49}$$

Let

$$h_n(Z_n)=f_n+s_n\psi_{n1}^2(\|x\|)+s_n\psi_{n2}^2\circ\bar{\alpha}_1^{-1}(v+D_0), \tag{50}$$

where $Z_n=[x^T,s_n,v]^T\in\mathbb{R}^{n+2}$. By using RBFNNs, the function $h_n(Z_n)$ can be approximated as

$$h_n(Z_n) = W_n^{*T}\Phi_n(Z_n) + \delta_n(Z_n), \tag{51}$$

Applying Young's inequality and Lemma 5, one has

$$s_n h_n(Z_n) \le \frac{1}{2a_n^2} s_n^2 \theta_n \Phi_n^T(X_n)\Phi_n(X_n) + \frac{a_n^2}{2}, \tag{52}$$

$$s_n \delta_n(Z_n) \le \frac{1}{2}s_n^2 + \frac{1}{2}\epsilon_n^2, \tag{53}$$

where $\theta_n = \|W_n^*\|^2$, $X_n = [x^T, s_n, v]^T$, and $\epsilon_n(\bar{s}_n^T, \bar{\hat{\theta}}_n^T, y_d, \dot{y}_d)$ is a continuous function satisfying $|\delta_n(Z_n)| \le \epsilon_n(\bar{s}_n^T, \bar{\hat{\theta}}_n^T, y_d, \dot{y}_d)$.

The actual control input u and the adaptive law $\hat{\theta}_n$ are designed as follows

$$\begin{aligned} u = \frac{1}{g_n}\Bigg[&- \frac{s_n}{2p_{n1}T_{cn1}} \exp\left(\left(\frac{1}{2}s_n^2\right)^{p_{n1}}\right)\left(\frac{1}{2}s_n^2\right)^{-p_{n1}} - \frac{\eta_n}{2p_{n3}T_{cn3}} \exp\left(\left(\frac{1}{2}\eta_n^2\right)^{p_{n3}}\right)\left(\frac{1}{2}\eta_n^2\right)^{-p_{n3}} \\ &- \frac{1}{2a_n^2}s_n\hat{\theta}_n\Phi_n^T\Phi_n - \frac{1}{2}s_n^2 - g_{n-1}s_{n-1} + \dot{\omega}_n\Bigg], \end{aligned} \tag{54}$$

$$\dot{\hat{\theta}}_n = -\frac{r_n}{p_{n2}T_{cn2}} \exp\left(\left(\frac{1}{2}\hat{\theta}_n^2\right)^{p_{n2}}\right)\left(\frac{1}{2}\hat{\theta}_n^2\right)^{\frac{1}{2}-p_{n2}}\hat{\theta}_n + \frac{1}{2a_n^2}s_n^2\Phi_n^T(X_n)\Phi_n(X_n), \tag{55}$$

where $a_n > 0, r_n > 0$ are positive design parameters.

By inserting (52)–(55) into (48), one has

$$\begin{aligned} \dot{V}_n \le &- \sum_{i=1}^{n} \frac{1}{p_{i1}T_{ci1}} \exp\left(\left(\frac{1}{2}s_i^2\right)^{p_{i1}}\right)\left(\frac{1}{2}s_i^2\right)^{1-p_{i1}} + \sum_{i=1}^{n} \frac{r_i\hat{\theta}_i\tilde{\theta}_i}{p_{i2}T_{ci2}} \exp\left(\left(\frac{1}{2}\hat{\theta}_i^2\right)^{p_{i2}}\right)\left(\frac{1}{2}\hat{\theta}_i^2\right)^{\frac{1}{2}-p_{i2}} \\ &+ \sum_{i=1}^{n}\frac{a_i^2}{2} + \sum_{i=1}^{n}\frac{1}{2}\epsilon_i^2 + \frac{n}{2} \end{aligned}. \tag{56}$$

Consider the overall Lyapunov function V defined by

$$V = V_n + \sum_{i=1}^{n}\frac{1}{2}\eta_i^2. \tag{57}$$

By utilizing (23) and (56) and differentiating (57), we obtain

$$\begin{aligned} \dot{V} &= \dot{V}_n + \sum_{i=1}^{n}\eta_i\dot{\eta}_i \\ &\le - \sum_{i=1}^{n} \frac{1}{p_{i1}T_{ci1}} \exp\left(\left(\tfrac{1}{2}s_i^2\right)^{p_{i1}}\right)\left(\tfrac{1}{2}s_i^2\right)^{1-p_{i1}} + \sum_{i=1}^{n} \frac{r_i\hat{\theta}_i\tilde{\theta}_i}{p_{i2}T_{ci2}} \exp\left(\left(\tfrac{1}{2}\hat{\theta}_i^2\right)^{p_{i2}}\right)\left(\tfrac{1}{2}\hat{\theta}_i^2\right)^{\frac{1}{2}-p_{i2}} \\ &\quad - \sum_{i=1}^{n} \frac{1}{p_{i3}T_{ci3}} \exp\left(\left(\tfrac{1}{2}\eta_i^2\right)^{p_{i3}}\right)\left(\tfrac{1}{2}\eta_i^2\right)^{1-p_{i3}} + \sum_{i=1}^{n}\left(\frac{a_i^2}{2} + \frac{\epsilon_i^2}{2}\right) + \sum_{i=1}^{n-1} g_i\eta_i(\omega_{i+1} - \alpha_i) \\ &\quad + \sum_{i=1}^{n-1} g_i\eta_i\eta_{i+1} + \frac{n}{2}. \end{aligned} \tag{58}$$

Observe that for all i, $\theta_i \ge 0$, $\hat{\theta}_i \ge 0$, and $\hat{\theta}_i\tilde{\theta}_i \le \frac{1}{2}\theta_i^2 - \frac{1}{2}\tilde{\theta}_i^2$. We continue the analysis by addressing the following two scenarios.

Case 1: Suppose $\tilde{\theta}_i \geq 0$ and $\hat{\theta}_i \geq 0$. Then, it holds that

$$\begin{aligned}
&\sum_{i=1}^{n} \exp\left(\left(\tfrac{1}{2}\hat{\theta}_i^2\right)^{p_{i2}}\right)\left(\tfrac{1}{2}\hat{\theta}_i^2\right)^{\frac{1}{2}-p_{i2}}\hat{\theta}_i\tilde{\theta}_i \\
&= \sum_{i=1}^{n} \exp\left(\left(\tfrac{1}{2}(\theta_i-\tilde{\theta}_i)^2\right)^{p_{i2}}\right)\left(\tfrac{1}{2}(\theta_i-\tilde{\theta}_i)^2\right)^{\frac{1}{2}-p_{i2}}\hat{\theta}_i\tilde{\theta}_i \\
&\leq \sum_{i=1}^{n} \exp\left(\left(\tfrac{1}{2}\theta_i^2+\tfrac{1}{2}\tilde{\theta}_i^2\right)^{p_{i2}}\right)\left(\tfrac{1}{2}\theta_i^2+\tfrac{1}{2}\tilde{\theta}_i^2\right)^{\frac{1}{2}-p_{i2}}\left(\tfrac{1}{2}\theta_i^2-\tfrac{1}{2}\tilde{\theta}_i^2\right) \\
&= \sum_{i=1}^{n} \exp\left(\left(\tfrac{1}{2}\theta_i^2+\tfrac{1}{2}\tilde{\theta}_i^2\right)^{p_{i2}}\right)\left(\tfrac{1}{2}\theta_i^2+\tfrac{1}{2}\tilde{\theta}_i^2\right)^{\frac{1}{2}-p_{i2}}\frac{1}{2}\theta_i^2 \\
&\quad - \sum_{i=1}^{n} \exp\left(\left(\tfrac{1}{2}\theta_i^2+\tfrac{1}{2}\tilde{\theta}_i^2\right)^{p_{i2}}\right)\left(\tfrac{1}{2}\theta_i^2+\tfrac{1}{2}\tilde{\theta}_i^2\right)^{\frac{1}{2}-p_{i2}}\frac{1}{2}\tilde{\theta}_i^2 \\
&\leq \sum_{i=1}^{n} \exp(\theta_i^{2p_{i2}})\theta_i^{3-2p_{i2}} - \sum_{i=1}^{n} \exp\left(\left(\tfrac{1}{2}\tilde{\theta}_i^2\right)^{p_{i2}}\right)\left(\tfrac{1}{2}\tilde{\theta}_i^2\right)^{\frac{3}{2}-p_{i2}}.
\end{aligned} \tag{59}$$

Case 2: Suppose $\tilde{\theta}_i < 0$, $\hat{\theta}_i \geq 0$. Then, it holds that

$$\begin{aligned}
\sum_{i=1}^{n} \exp\left(\left(\tfrac{1}{2}\hat{\theta}_i^2\right)^{p_{i2}}\right)\left(\tfrac{1}{2}\hat{\theta}_i^2\right)^{\frac{1}{2}-p_{i2}}\hat{\theta}_i\tilde{\theta}_i &\leq - \sum_{i=1}^{n} \exp\left(\left(\tfrac{1}{2}\hat{\theta}_i^2\right)^{p_{i2}}\right)\left(\tfrac{1}{2}\hat{\theta}_i^2\right)^{\frac{1}{2}-p_{i2}}\tilde{\theta}_i^2 \\
&\leq - \sum_{i=1}^{n} \exp\left(\left(\tfrac{1}{2}\tilde{\theta}_i^2\right)^{p_{i2}}\right)\left(\tfrac{1}{2}\tilde{\theta}_i^2\right)^{\frac{3}{2}-p_{i2}}.
\end{aligned} \tag{60}$$

From cases 1 and 2, one has

$$\begin{aligned}
&\sum_{i=1}^{n} \exp\left(\left(\tfrac{1}{2}\hat{\theta}_i^2\right)^{p_{i2}}\right)\left(\tfrac{1}{2}\hat{\theta}_i^2\right)^{\frac{1}{2}-p_{i2}}\hat{\theta}_i\tilde{\theta}_i \leq - \sum_{i=1}^{n} \exp\left(\left(\tfrac{1}{2}\tilde{\theta}_i^2\right)^{p_{i2}}\right)\left(\tfrac{1}{2}\tilde{\theta}_i^2\right)^{\frac{3}{2}-p_{i2}} \\
&+ \sum_{i=1}^{n} \exp(\theta_i^{2p_{i2}})\theta_i^{3-2p_{i2}}.
\end{aligned} \tag{61}$$

Based on $|h(x,y)x^m y^n| \leq \frac{n}{m+n}\left(\frac{m}{(m+n)c(x,y)}\right)^{\frac{m}{n}}|h(x,y)|^{\frac{m+n}{n}} + c(x,y)|y|^{m+n}$, for $m,n \in \mathbb{R}^+$, $x,y \in \mathbb{R}$, $c(x,y) > 0$, one has

$$\begin{aligned}
&\sum_{i=1}^{n} \exp\left(\left(\tfrac{1}{2}\tilde{\theta}_i^2\right)^{p_{i2}}\right)\left(\tfrac{1}{2}\tilde{\theta}_i^2\right)^{1-p_{i2}} \leq \sum_{i=1}^{n} \frac{1}{p_{i2}T_{ci2}} \exp\left(\left(\tfrac{1}{2}\tilde{\theta}_i^2\right)^{p_{i2}}\right)\left(\tfrac{1}{2}\tilde{\theta}_i^2\right)^{\frac{3}{2}-p_{i2}} \\
&+ \sum_{i=1}^{n} \exp\left(\theta_i^{2p_{i2}}\right)\Theta_i,
\end{aligned} \tag{62}$$

where $\Theta_i = \frac{2-2p_{i2}}{3-2p_{i2}}\left(\frac{p_{i2}T_{ci2}}{3-2p_{i2}}\right)^{\frac{1}{2}(1-p_{i2})}$.

By using (61), (62) with the inequality $f_{k_1}(x) = \exp(x^{k_1})x^{1-k_1} \leq f_{k_2}(x) = \exp(x^{k_2})x^{1-k_2}$, for $0 < k_1 < k_2 \leq 1$, $x \geq 0$, one has

$$\begin{aligned}
\dot{V} \leq &- \sum_{i=1}^{n} \frac{1}{p_{i1}T_{ci1}} \exp\left(\left(\tfrac{1}{2}s_i^2\right)^{p_m}\right)\left(\tfrac{1}{2}s_i^2\right)^{1-p_m} - \sum_{i=1}^{n} \frac{r_i}{p_{i2}T_{ci2}} \exp\left(\left(\tfrac{1}{2}\tilde{\theta}_i^2\right)^{p_m}\right)\left(\tfrac{1}{2}\tilde{\theta}_i^2\right)^{1-p_m} \\
&- \sum_{i=1}^{n} \frac{1}{p_{i3}T_{ci3}} \exp\left(\left(\tfrac{1}{2}\eta_i^2\right)^{p_m}\right)\left(\tfrac{1}{2}\eta_i^2\right)^{1-p_m} + \sum_{i=1}^{n} \frac{1}{2}\epsilon_i^2 \\
&+ \sum_{i=1}^{n-1} g_i\eta_i(\omega_{i+1}-\alpha_i) + \sum_{i=1}^{n-1} g_i\eta_i\eta_{i+1} + \mu,
\end{aligned} \tag{63}$$

where $p_m = \min\{p_{11}, \ldots, p_{n3}\}$ and $\mu = \sum_{i=1}^{n} \exp(\theta_i^{2p_{i2}})\Theta_i + \sum_{i=1}^{n} \frac{\theta_i^{3-2p_{i2}}}{p_{i2}T_{ci2}} \exp(\theta_i^{2p_{i2}}) + \sum_{i=1}^{n} \frac{a_i^2}{2} + \frac{n}{2}$.

From Lemma 4, one has

$$\begin{aligned}
&\sum_{i=1}^{n} \exp\left(\left(\tfrac{1}{2}s_i^2\right)^{p_m}\right)\left(\tfrac{1}{2}s_i^2\right)^{1-p_m} + \sum_{i=1}^{n} \exp\left(\left(\tfrac{1}{2}\tilde{\theta}_i^2\right)^{p_m}\right)\left(\tfrac{1}{2}\tilde{\theta}_i^2\right)^{1-p_m} \\
&\quad + \sum_{i=1}^{n} \exp\left(\left(\tfrac{1}{2}\eta_i^2\right)^{p_m}\right)\left(\tfrac{1}{2}\eta_i^2\right)^{1-p_m} \\
&\geq \frac{1}{3n}\left\{\sum_{i=1}^{n}\left[\exp\left(\left(\tfrac{1}{2}s_i^2\right)^{p_m}\right) + \exp\left(\left(\tfrac{1}{2}\tilde{\theta}_i^2\right)^{p_m}\right) + \exp\left(\left(\tfrac{1}{2}\eta_i^2\right)^{p_m}\right)\right]\right\} \\
&\quad \times \left\{\sum_{i=1}^{n}\left[\left(\tfrac{1}{2}s_i^2\right)^{1-p_m} + \left(\tfrac{1}{2}\tilde{\theta}_i^2\right)^{1-p_m} + \left(\tfrac{1}{2}\eta_i^2\right)^{1-p_m}\right]\right\}.
\end{aligned} \tag{64}$$

Next, using the inequality $\left(\prod_{k=1}^{m} x_k\right)^{1/m} \leq \frac{1}{m}\sum_{k=1}^{m} x_k, x_k \in \mathbb{R}_{\geq 0}$, and $\left(\sum_{k=1}^{m} \|y_k\|\right)^p \leq \sum_{k=1}^{m} \|y_k\|^p, p \in [0,1], y_k \in \mathbb{R}$, one has

$$\begin{aligned}
&\frac{1}{3n}\left\{\sum_{i=1}^{n}\left[\exp\left(\left(\tfrac{1}{2}s_i^2\right)^{p_m}\right) + \exp\left(\left(\tfrac{1}{2}\tilde{\theta}_i^2\right)^{p_m}\right) + \exp\left(\left(\tfrac{1}{2}\eta_i^2\right)^{p_m}\right)\right]\right\} \\
&\geq \exp\left(\frac{1}{3n}\sum_{i=1}^{n}\left(\tfrac{1}{2}s_i^2 + \tfrac{1}{2}\tilde{\theta}_i^2 + \tfrac{1}{2}\eta_i^2\right)^{p_m}\right).
\end{aligned} \tag{65}$$

Moreover, by using $\left(\sum_{k=1}^{m} \|y_k\|\right)^p \leq \sum_{k=1}^{m} \|y_k\|^p, p \in [0,1], y_k \in \mathbb{R}$, one has

$$\sum_{i=1}^{n}\left(\left(\tfrac{1}{2}s_i^2\right)^{1-p_m} + \left(\tfrac{1}{2}\tilde{\theta}_i^2\right)^{1-p_m} + \left(\tfrac{1}{2}\eta_i^2\right)^{1-p_m}\right) \geq \left(\sum_{i=1}^{n}\left(\tfrac{1}{2}s_i^2 + \tfrac{1}{2}\tilde{\theta}_i^2 + \tfrac{1}{2}\eta_i^2\right)\right)^{1-p_m}. \tag{66}$$

We now proceed with the stability analysis of the closed-loop system. Define the following compact set

$$\Omega = \left\{\left[\bar{s}_n^T, \bar{\tilde{\theta}}_n^T, \bar{\eta}_n^T\right]^T : V \leq P\right\}, \tag{67}$$

where $P > 0$ is an arbitrarily specified constant.

Theorem 1. *Let us consider the nonlinear system governed by Equation (1), controlled using the input defined in Equation (54). The associated virtual control signals are formulated as in Equations (32) and (43), while the adaptive parameter update laws are provided in Equations (33), (44), and (55). Suppose that all the required assumptions and conditions mentioned earlier are fulfilled. Then, for any initial condition satisfying $V(0) \leq P$, where $P > 0$ is a user-defined constant, the resulting closed-loop system is guaranteed to be predefined-time-bounded. In particular, every signal within the system remains bounded and converges to a small vicinity of the equilibrium point within a fixed time T_c, which satisfies the inequality $T_c \leq \frac{1}{\alpha\beta p_m}$, where α and β are positive constants. The design parameters p_{ik} and T_{cik} are chosen to ensure that*

$$\begin{cases}
\frac{1}{p_{i1}T_{ci1}} \geq \alpha, \\
\frac{1}{p_{i3}T_{ci3}} \geq \alpha, \\
\alpha = \min\left\{\frac{r_i}{p_{i2}T_{ci2}}\right\}, \quad i = 1, \ldots, n.
\end{cases} \tag{68}$$

Proof. Suppose that $V \leq P$. Under this condition, it follows that the signals s_i, $\hat{\theta}_i$, and η_i are all bounded for $i = 1, \ldots, n$. As a result, the variable $z_i = s_i + \eta_i$ is also bounded. Given

that the reference signal y_d belongs to L_∞, (20) implies that the system output $y = x_1$ is also in L_∞, which further leads to the conclusion that the auxiliary signal v is bounded. From (32), we can deduce that α_1 remains bounded. Applying (21), it follows that both ω_2 and its time derivative $\dot{\omega}_2$ are bounded, which implies that α_2 is also bounded. Proceeding in the same manner for higher-order subsystems ($i = 3, \ldots, n-1$), it can be established that α_i, ω_i, and $\dot{\omega}_i$ are bounded. Furthermore, it is evident that ω_n, $\dot{\omega}_n$, and the control input u are all bounded. Therefore, each state variable $x_i = z_i + \omega_i$ is bounded for $i = 2, \ldots, n$, i.e., $x_i \in L_\infty$. Hence, there exists a constant $C > 0$ such that the following inequality holds $\sum_{i=1}^{n-1} g_i \eta_i \eta_{i+1} + \sum_{i=1}^{n-1} g_i \eta_i (\omega_{i+1} - \alpha_i) \leq C$. Moreover, the continuous functions ϵ_i ($i = 1, \ldots, n$) attain upper bounds N_i over the compact set $\Omega \times \Omega_d$.

By using (63)–(66) and (68), one has

$$\begin{aligned}
\dot{V} &\leq -\alpha \exp\left(\frac{1}{3n}\sum_{i=1}^{n}\left(\frac{1}{2}s_i^2 + \frac{1}{2}\tilde{\theta}_i^2 + \frac{1}{2}\eta_i^2\right)^{p_m}\right)\left[\sum_{i=1}^{n}\left(\frac{1}{2}s_i^2 + \frac{1}{2}\tilde{\theta}_i^2 + \frac{1}{2}\eta_i^2\right)\right]^{1-p_m} \\
&\quad + \sum_{i=1}^{n}\frac{1}{2}N_i + C + \mu \\
&\leq -\alpha \exp\left(\frac{1}{3n}V^{p_m}\right)V^{1-p_m} + \sum_{i=1}^{n}\frac{1}{2}N_i + C + \mu, \\
&\leq -\frac{\alpha_0}{p_m}\exp(\beta V^{p_m})V^{1-p_m} + D,
\end{aligned} \tag{69}$$

where $\alpha_0 = \alpha p_m$, $\beta = \frac{1}{3n}$, and $D = \sum_{i=1}^{n}\frac{1}{2}N_i + C + \mu$.

Since $\frac{D}{\exp(\beta P^{p_m})P^{1-p_m}} < \frac{D}{P^{1-p_m}}$, it follows that $\dot{V} < 0$ when $V = P$, provided that $\alpha > \frac{D}{P^{1-p_m}}$. Therefore, if the initial condition satisfies $V(0) \leq P$, then $\dot{V}(t) \leq 0$ for all $t \geq 0$. Given any positive constant P and any set of design parameters p_{ik} and T_{cik}, one can always select r_i sufficiently large to ensure that $\alpha > \frac{D}{P^{1-p_m}}$, since D is independent of r_i. As a result, all closed-loop signals remain bounded, and the system states converge to an arbitrarily small neighborhood of the origin within a predefined time $T_c \leq \frac{1}{\alpha\beta p_m}$. This completes the proof. □

Remark 4. *In the proposed control design, the number of nodes in the radial basis function approximation is selected according to the expected variation of the nonlinear function to be approximated. Functions exhibiting stronger nonlinear behavior require more nodes to capture their characteristics, whereas smoother functions can be represented adequately with fewer nodes. This choice ensures that the approximation quality remains sufficient for the stability analysis. The approximation error enters the closed-loop system as a bounded term, and its upper bound directly influences the size of the convergence vicinity of the tracking error. A smaller approximation error yields a tighter convergence region, while a larger error leads to a slightly wider neighborhood around the desired trajectory. Nonetheless, the predefined-time ultimate boundedness of all closed-loop signals is preserved.*

Remark 5. *The dynamic signal $v(t)$ is introduced to mitigate the influence of the unmodeled dynamics $\dot{\xi} = q(t, \xi, x)$. Its design allows the controller to remain robust even when the characteristics of $q(t, \xi, x)$ vary in magnitude or rate. Specifically, the boundedness assumptions on $q(t, \xi, x)$ ensure that any variation in its time constant or amplitude appears as a bounded disturbance in the closed-loop system. The adaptive laws and predefined-time stability framework compensate for these effects, so larger variations in $q(t, \xi, x)$ may enlarge the ultimate convergence region but do not compromise stability. Conversely, smaller variations lead to improved tracking accuracy. This provides inherent robustness to different forms of unmodeled dynamics while preserving predefined-time ultimate boundedness.*

Remark 6. *The parameters p_{i1} and T_{ci1} play a key role in determining the predefined-time convergence behavior. The constant T_{ci1} appears in the predefined-time term and sets the upper bound of the settling time T_c. Choosing a smaller T_{ci1} leads to faster convergence, whereas a larger value results in a slower transient response. The parameter p_{i1} influences the shape of the transient phase by regulating how quickly the predefined-time term increases as the error evolves. Smaller values of p_{i1} produce more aggressive error decay, while values closer to one yield a smoother response.*

Remark 7. *In contrast to the existing studies [30,49,57], the present work tackles a broader and more demanding problem setting where nonstrict-feedback nonlinear systems are simultaneously affected by input delay, input saturation, and unmodeled dynamics. These factors, when combined, significantly complicate the controller design and stability analysis. To manage these challenges, a refined command-filter-based adaptive structure is developed, which avoids the repeated differentiation of virtual control laws and reduces the number of adaptive parameters involved in the design. This not only lowers the computational burden but also simplifies implementation in practical applications. Furthermore, the proposed method ensures fixed-time tracking performance under all considered nonlinearities, which enhances its applicability. These features collectively form the distinguishing aspects of this manuscript compared with the referenced works.*

Figure 1 illustrates the complete architecture of the proposed adaptive control scheme through a detailed block diagram.

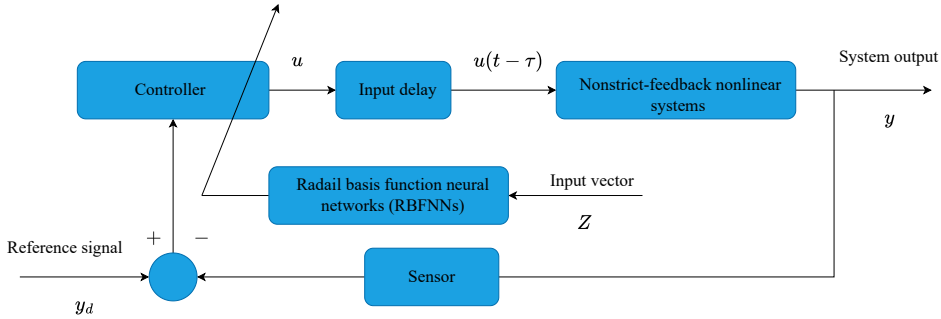

Figure 1. Block diagram illustrating the complete structure of the proposed adaptive control scheme.

4. Simulation Results

This section validates the performance of the proposed adaptive controller through two illustrative simulation examples.

Example 1 (Numerical example). *We examine a nonlinear system represented in nonstrict-feedback form, given by*

$$\begin{cases} \dot{\xi} = -\xi + 0.25x_1^2 + 0.3, \\ \dot{x}_1 = x_2(1.5 + 0.5\sin(x_1)) + x_1x_2 + x_2\sin(x_2) + \xi x_1\sin(x_1), \\ \dot{x}_2 = u(t-\tau)(1.5 + \sin(x_1x_2)) + x_1x_2e^{x_2} + x_1x_2\xi, \\ y = x_1, \end{cases} \tag{70}$$

where $g_1 = 1.5 + 0.5\sin(x_1))$, $g_2 = 1.5 + \sin(x_1x_2)$, $f_1 = x_1x_2 + x_2\sin(x_2)$, $f_2 = x_1x_2e^{x_2}$, $q(t,\xi,x) = -\xi + 0.25x_1^2 + 0.3$, $\Delta_1 = \xi x_1\sin(x_1)$, $\Delta_2 = x_1x_2\xi$. The desired trajectory is defined as $y_d = 0.5\sin(t)$, and the input delay is set to $\tau = 0.02$. To construct the dynamic signal v, we utilize Equation (4) and select the Lyapunov candidate as $V(\xi) = \xi^2$. The associated class $\mathcal{K}_\infty$ functions are chosen as $\bar{\alpha}_1(\|\xi\|) = 0.5\xi^2$ and $\bar{\alpha}_2(\|\xi\|) = 2\xi^2$. From (5), the derivative of $V(\xi)$ with respect to time satisfies

$$\begin{aligned}\frac{\partial V(\xi)}{\partial \xi} q(t,\xi,x) &= 2\xi(-\xi + 0.2x_1^2 + 0.3) \\ &\leq -2\xi^2 + 0.4|x_1|^2|\xi| + 0.6|\xi| \\ &\leq -1.6\xi^2 + 2.5x_1^4 + 0.5, \end{aligned} \tag{71}$$

where we let $c = 1.6$, $\gamma(|x_1|) = 2.5x_1^4$, *and* $d = 0.5$. *For design purposes, we select* $c = 1.5$ *and* $\bar{\gamma}(|x_1|) = 1.5x_1^4$, *leading to the dynamic signal*

$$\dot{v} = -1.5\xi^2 + 1.5x_1^4 + 0.5. \tag{72}$$

Based on Theorem 1, the real control input u defined in (54) for the case $n = 2$, the virtual control law α_1 defined in (32), the adaptive laws $\hat{\theta}_i$ defined in (44) for $i = 1, 2$, and the compensating signals η_1 and η_2 defined in (23) are selected for implementation. The centers and widths of the RBFNN are chosen uniformly over compact sets. Specifically, the neural network $W_1^{*T}\Phi_1(Z_1)$ employs three nodes with centers evenly distributed in $[-5,\ 5]$ and width set to 2. The neural network $W_2^{*T}\Phi_2(Z_2)$ uses nine nodes with centers uniformly spaced in $[-5,\ 5] \times [-5,\ 5]$, also with a width of 2. The initial conditions are specified as $[x_1(0),\ x_2(0)]^T = [0.5,\ 0.5]^T$, $[\hat{\theta}_1(0),\ \hat{\theta}_2(0)]^T = [0,\ 0]^T$, and $[\eta_1(0),\ \eta_2(0)]^T = [0.05,\ 0.15]^T$, with $v(0) = 0$ and $\xi(0) = 0$. The design parameters are chosen as $p_{11} = p_{12} = p_{13} = p_{21} = p_{22} = p_{23} = 0.2$, $T_{c_{11}} = T_{c_{12}} = T_{c_{13}} = T_{c_{21}} = T_{c_{22}} = T_{c_{23}} = 0.4$, $\tau_2 = 0.02$, $r_1 = r_2 = 0.8$, and $a_1 = a_2 = 1.5$.

The effectiveness of the proposed predefined-time adaptive control strategy is demonstrated through simulation results shown in Figures 2–7. In Figure 2, the system output y is compared with the reference signal y_d, revealing accurate trajectory tracking. The tracking error e, illustrated in Figure 3, converges quickly to a small neighborhood around zero, indicating the rapid and precise tracking performance of the controller. Figure 4 presents the time evolution of the system state x_2, which remains stable and bounded under the implemented control law. Figures 5 and 6 display the actual control input u and the estimated parameters $\hat{\theta}_1$ and $\hat{\theta}_2$, respectively, both of which remain within bounded limits, thereby verifying the robustness of the control and adaptation mechanisms. Figure 7 shows the trajectories of ξ and v, further supporting the stability of internal signals. Overall, the simulation results confirm that all closed-loop signals are bounded and that the tracking error reaches a small vicinity of the origin within the specified predefined time.

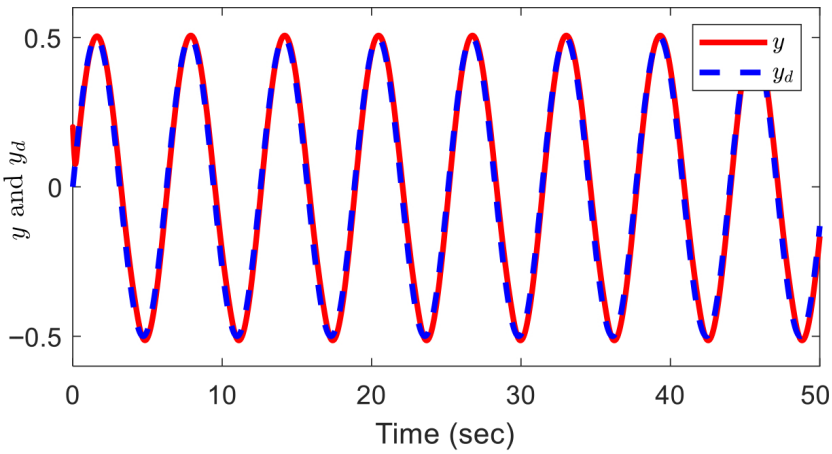

Figure 2. Response of the system output y in comparison with the desired reference trajectory y_d.

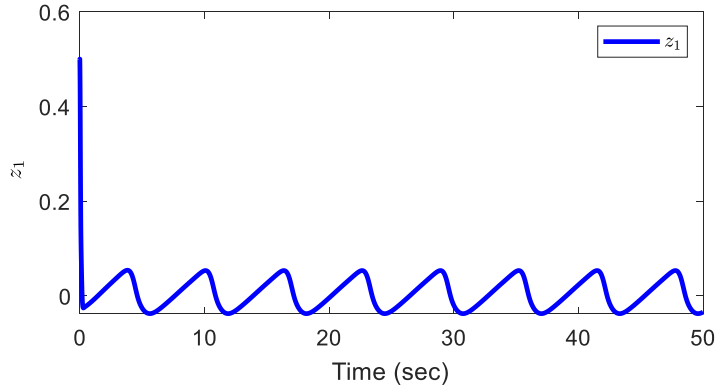

Figure 3. Evolution of the tracking error z_1.

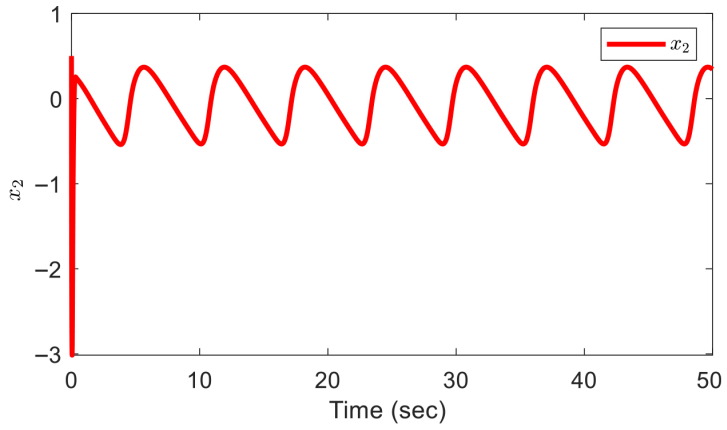

Figure 4. Time response of the system state variable x_2.

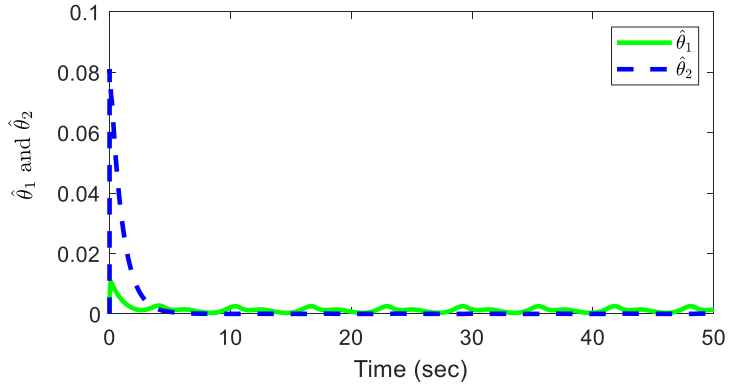

Figure 5. Adaptive parameter $\hat{\theta}_1$ and $\hat{\theta}_2$.

To demonstrate the effectiveness of the proposed predefined-time control scheme, a comparative analysis is conducted against an existing fixed-time control scheme [42]. Both control strategies employ command filter techniques to reduce computational complexity. The comparison is based on widely used performance indices [28].

- **Integral Square Error (ISE)**:

$$\text{ISE} = \sum_{k} e_1^T(k) e_1(k)$$

- **Integral Absolute Error (IAE)**:

$$\text{IAE} = \sum_{k}\sum_{i}|e_{1i}(k)|$$

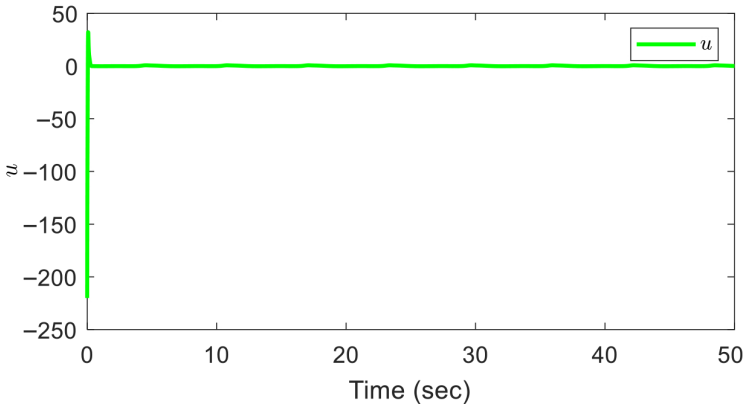

Figure 6. Trajectory of control input u.

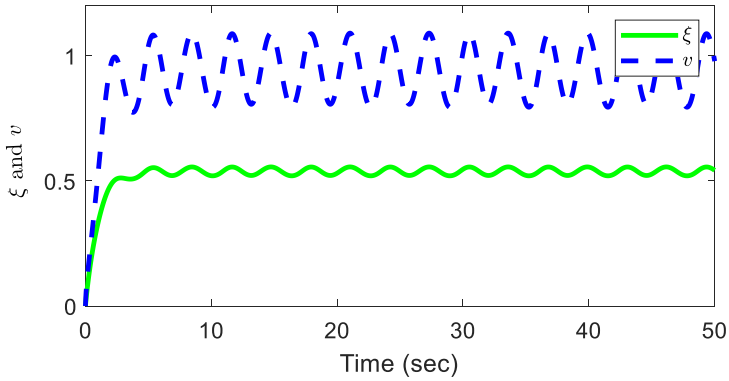

Figure 7. Dynamic behavior of ξ and v.

Table 1 presents the quantitative comparison of both control schemes using the above indices.

Table 1. Comparison of performance metrics between the proposed predefined-time controller and the fixed-time controller from [42] for Example 1.

Performance Index	Proposed Predefined-Time Controller	Fixed-Time Controller [42]
ISE	6.9372	7.2845
IAE	54.6193	58.1027

As shown in Table 1, the predefined-time control scheme yields slightly better performance than the fixed-time counterpart [42]. The reduced values of ISE and IAE indicate enhanced tracking precision and faster convergence, thereby validating the superiority and practicality of the proposed approach.

In addition to the numerical comparison, the tracking error z_1 responses of both methods are illustrated in Figure 8 to further enhance the persuasiveness and intuitiveness of the results. As observed, the predefined-time control scheme exhibits slightly better performance than the fixed-time counterpart [42], since the tracking error under the proposed method shows smaller fluctuations and smoother convergence. Figure 8 clearly demonstrates the improved transient behavior and tighter error bounds achieved by the proposed predefined-time controller.

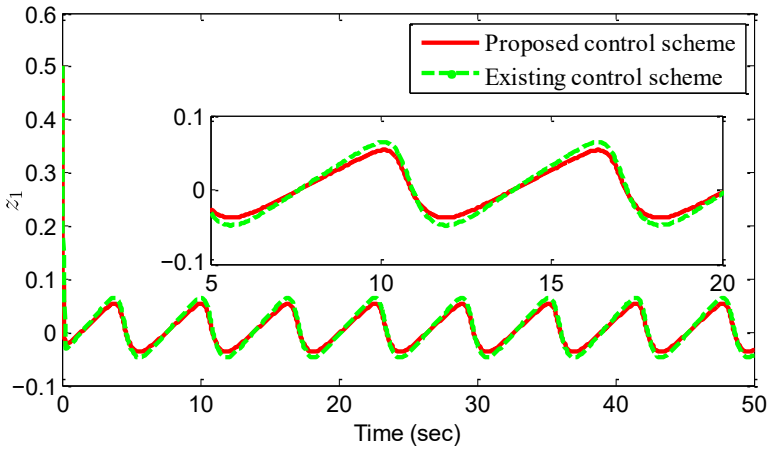

Figure 8. Trajectory of the tracking error z_1 under the proposed method and the existing method [42].

Comparison under different initial conditions: To highlight the robustness of the proposed predefined-time controller for Example 1, additional simulations are performed under three different sets of initial system conditions. The tracking performance of both the proposed controller and the fixed-time controller [42] is evaluated using the integral square error (ISE) and the integral absolute error (IAE). The initial conditions for the three cases are:

- **IC1:** $[x_1(0),\, x_2(0)]^T = [0.5,\, 0.5]^T$
- **IC2:** $[x_1(0),\, x_2(0)]^T = [-0.4,\, 0.6]^T$
- **IC3:** $[x_1(0),\, x_2(0)]^T = [0.3,\, -0.5]^T$

The quantitative comparison under these conditions is summarized in Table 2.

Table 2. Comparison of performance indices between the proposed predefined-time controller and the fixed-time controller [42] under different initial conditions for Example 1.

Performance Index	IC1	IC2	IC3
Proposed ISE	6.9372	7.1048	6.8253
Fixed-time ISE [42]	7.2845	7.5631	7.2197
Proposed IAE	54.6193	56.2041	53.4872
Fixed-time IAE [42]	58.1027	59.8749	57.3165

The results show that the proposed predefined-time controller consistently yields smaller ISE and IAE values across all initial conditions, indicating better transient response and reduced error accumulation compared to the fixed-time controller [42].

Comparison under different predefined times: To demonstrate the adjustability and effectiveness of the proposed predefined-time controller, simulations were performed for three different values of the predefined convergence times, $T_{c_i} = 0.4$, 0.8, and 1.2 s. The performance was evaluated using the integral square error (ISE) and integral absolute error (IAE).

From Table 3, it can be observed that the tracking error remains within a small neighborhood of zero for all cases, and the proposed controller successfully achieves convergence within the specified T_{c_i}. While increasing T_{c_i} slightly affects the error metrics, the overall tracking performance remains accurate and stable. These results confirm that the proposed predefined-time control scheme allows the convergence time to be explicitly prescribed and effectively realized in practice.

Table 3. Comparison of performance indices under different predefined times T_{c_i} for Example 1.

Performance Index	$T_{c_i} = 0.4$	$T_{c_i} = 0.8$	$T_{c_i} = 1.2$
ISE	6.9372	6.9815	7.0241
IAE	54.6193	55.1027	55.4876

Example 2 (Practical example). *The effectiveness of the proposed control strategy is evaluated using the electromechanical system shown in Figure 9, governed by [7]*

$$\begin{cases} M\ddot{q} + N\sin(q) + B\dot{q} = I + \tilde{I}, \\ L\dot{I} = -RI - K_B\dot{q} + V, \\ y = q, \end{cases} \tag{73}$$

where q, $\dot{q}$, and $\ddot{q}$ correspond to the angular displacement, angular velocity, and angular acceleration, respectively. The term I denotes the armature current of the motor, while $\tilde{I}$ accounts for disturbances affecting the current. The variable V represents the input control voltage. Additional descriptions and physical interpretations of the remaining system parameters are provided in [7].

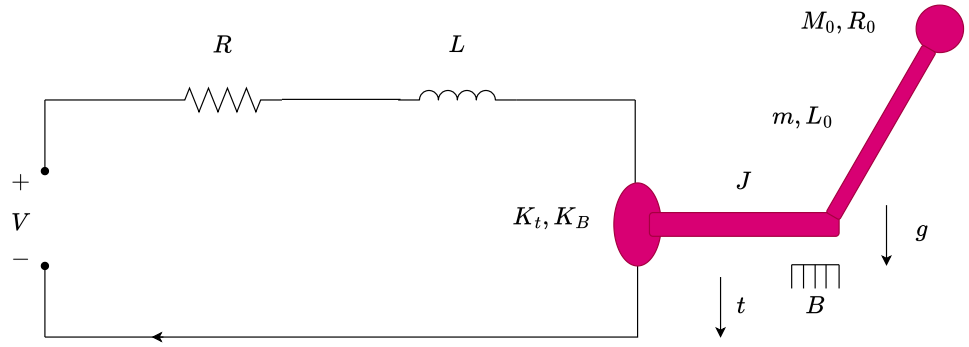

Figure 9. Framework of the electromechanical system.

Define the new state variables as $x_1 = q$, $x_2 = \dot{q}$, $x_3 = I$, and control input $u = V$. The system can be reformulated in a state-space representation as follows

$$\begin{cases} \dot{\xi} = -\xi + 0.3x_1^2 + 0.25 \\ \dot{x}_1 = x_2, \\ \dot{x}_2 = \dfrac{1}{M}x_3 - \dfrac{N}{M}\sin(x_1) - \dfrac{B}{M}x_2 + \dfrac{\tilde{I}}{M} + \xi x_2\cos(x_1), \\ \dot{x}_3 = \dfrac{1}{L}u(t-\tau) - \dfrac{R}{L}x_3 - \dfrac{K_B}{L}x_2 + 0.5\xi x_1 x_2\sin(x_3), \\ y = x_1. \end{cases} \tag{74}$$

where $g_1 = 1$, $g_2 = \dfrac{1}{\bar{M}}$, $g_3 = \dfrac{1}{L}$, $f_1 = 0$, $f_2 = -\dfrac{\bar{N}}{\bar{M}}\sin(x_1) - \dfrac{\bar{B}}{\bar{M}}x_2 + \dfrac{\tilde{I}}{\bar{M}}$, $f_3 = -\dfrac{R}{L}x_3 - \dfrac{K_B}{L}x_2 + 0.5\xi x_1 x_2\sin(x_3)$, $\Delta_1 = 0$, $\Delta_2 = \xi x_2\cos(x_1)$, $\Delta_3 = 0.5\xi x_1 x_2\sin(x_3)$, $q(t,\xi,x) = -\xi + 0.3x_1^2 + 0.25$. The parameters for simulation are selected as $N = 10$, $B = 1$, $M = 1$, $L = 0.05$, $K_B = 0.5$, and $R = 0.5$. The current disturbance is modeled as $\tilde{I} = 0.1x_1\sin(x_2x_3)$. The desired trajectory is chosen as $y_d = 0.5(\sin(t) + \sin(0.5t))$, and the input delay is set to $\tau = 0.02$. Employing a design methodology analogous to that used in Example 1, the dynamic signal is constructed as $\dot{v} = -1.2\xi^2 + 2.5x_1^4 + 0.625$.

Based on Theorem 1, the real control input u defined in (54) for the case $n = 3$, the virtual control law α_i defined in (43), the adaptive laws $\hat{\theta}_i$ defined in (44) for $i = 1, 2$, and

the compensating signals η_1, η_2, and η_3 defined in (23) are selected for implementation. The centers and widths of the RBFNNs are selected uniformly over compact sets. Specifically, the neural network $W_1^{*T}\Phi_1(Z_1)$ employs three nodes with centers evenly distributed in $[-5,\ 5]$ and width set to 2. The neural network $W_2^{*T}\Phi_2(Z_2)$ uses nine nodes with centers uniformly spaced in $[-5,\ 5] \times [-5,\ 5]$, also with width 2. For the third layer, the neural network $W_3^{*T}\Phi_3(Z_3)$ employs 27 nodes with centers arranged uniformly in $[-5,\ 5]^3$ and width again set to 2. The design parameters are selected as $p_{11} = p_{12} = p_{13} = p_{21} = p_{22} = p_{23} = p_{31} = p_{32} = p_{33} = 0.2$, $T_{c_{11}} = T_{c_{12}} = T_{c_{13}} = T_{c_{21}} = T_{c_{22}} = T_{c_{23}} = T_{c_{31}} = T_{c_{32}} = T_{c_{33}} = 0.4$, $\tau_2 = \tau_3 = 0.02$, $r_1 = r_2 = r_3 = 0.8$, and $a_1 = a_2 = a_3 = 1.5$. The initial conditions are set as $[x_1(0), x_2(0), x_3(0)]^T = [0.5, 0.5, 0.5]^T$, $[\hat{\theta}_1(0), \hat{\theta}_2(0), \hat{\theta}_3(0)]^T = [0, 0, 0]^T$, $[\eta_1(0), \eta_2(0), \eta_3(0)]^T = [0.05, -0.05, 0.1]^T$, with $v(0) = 0$ and $\xi(0) = 0$.

To demonstrate the performance of the proposed predefined-time adaptive control approach, simulation outcomes are illustrated in Figures 10–15. In Figure 10, the system output y is compared with the reference signal y_d, revealing accurate and precise trajectory tracking under the designed controller. Figure 11 shows the tracking error e, which quickly converges to a small vicinity around zero, verifying the fast response characteristic of the predefined-time control method. The system state variables x_2 and x_3 are plotted in Figure 12, indicating that the system remains stable and its states are well-contained throughout the control process. Figures 13 and 14 illustrate the applied control input u and the estimates of the unknown parameters $\hat{\theta}_1$, $\hat{\theta}_2$, and $\hat{\theta}_3$, respectively, all of which stay within bounded limits. Figure 15 depicts the trajectories of the internal signals ξ and v, further confirming the boundedness of the adaptive dynamics. The overall results confirm that all closed-loop signals remain uniformly bounded and that the tracking error approaches a small region near the origin within a predetermined time. This demonstrates the robustness and practical viability of the proposed control methodology.

To provide additional evidence of the proposed control strategy's effectiveness, a comparative performance analysis is conducted for Example 2. This comparison involves the proposed predefined-time control approach and the fixed-time control method presented in [42], with both schemes incorporating command filters. The evaluation relies on the ISE and IAE performance metrics previously introduced in Example 1.

As shown in Table 4, the proposed predefined-time control scheme outperforms the fixed-time approach [42] in terms of both accuracy and convergence. The lower ISE and IAE values demonstrate that the predefined-time strategy achieves more precise tracking with faster convergence, while ensuring that all closed-loop signals remain bounded. These results confirm the robustness and improved performance of the proposed control method in handling the one-link robotic manipulator system.

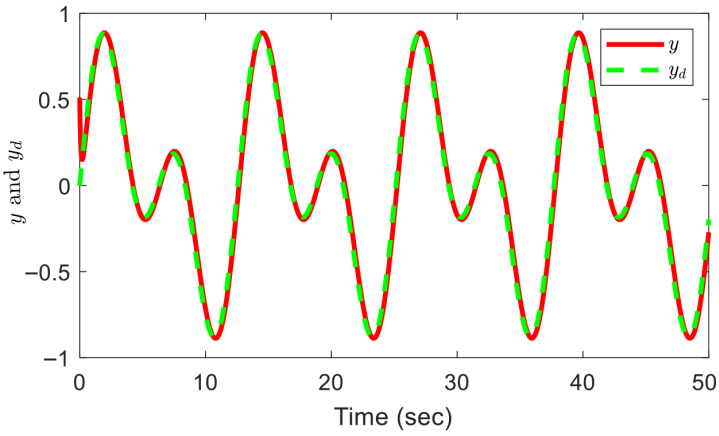

Figure 10. Response of the system output y in comparison with the desired reference trajectory y_d.

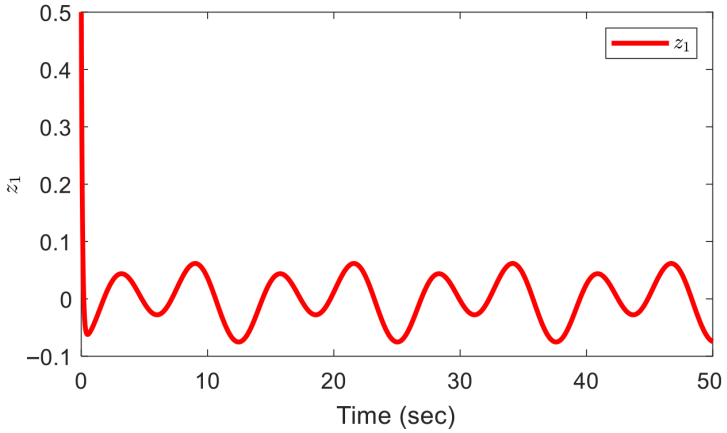

Figure 11. Evolution of the tracking error z_1.

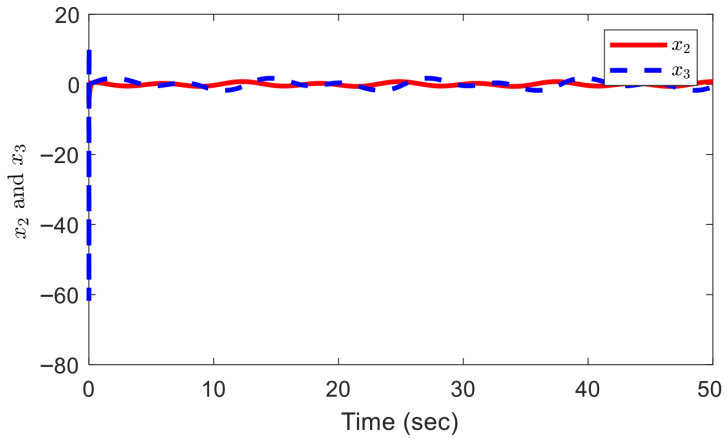

Figure 12. Time response of the system states x_2 and x_3.

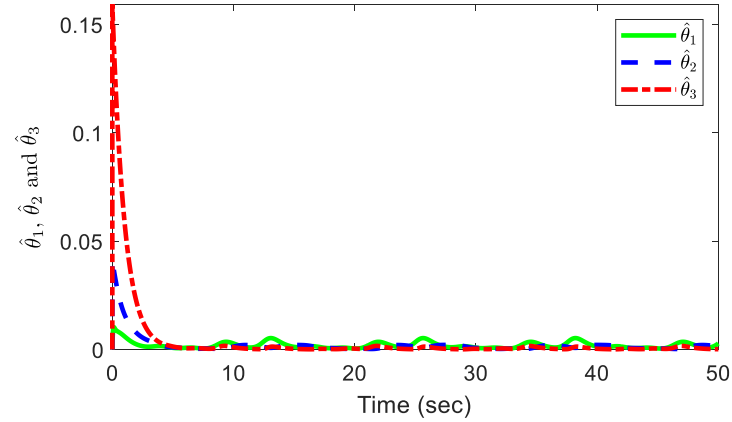

Figure 13. Adaptive parameter estimates $\hat{\theta}_1$, $\hat{\theta}_2$ and $\hat{\theta}_3$.

Table 4. Comparison of performance indices between the proposed predefined-time controller and the fixed-time controller presented in [42] for Example 2.

Performance Index	Proposed Predefined-Time Controller	Fixed-Time Controller [42]
ISE	26.4825	28.7154
IAE	322.9997	339.4872

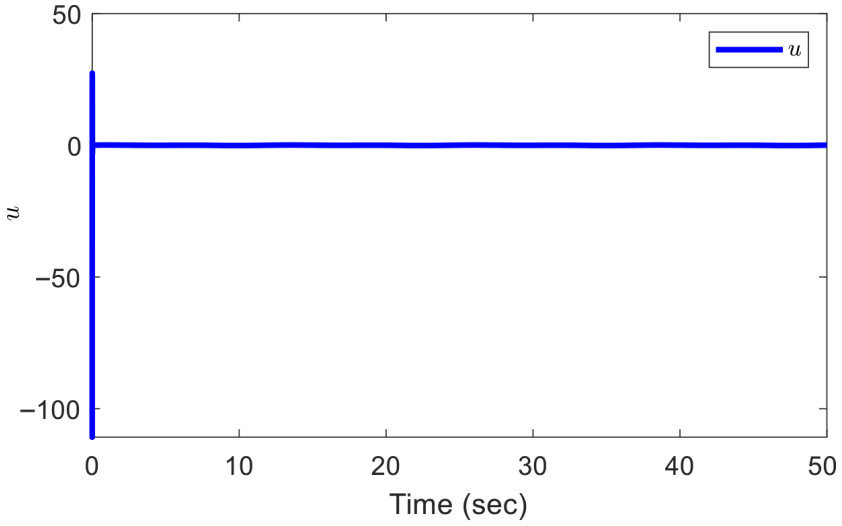

Figure 14. Trajectory of control input u.

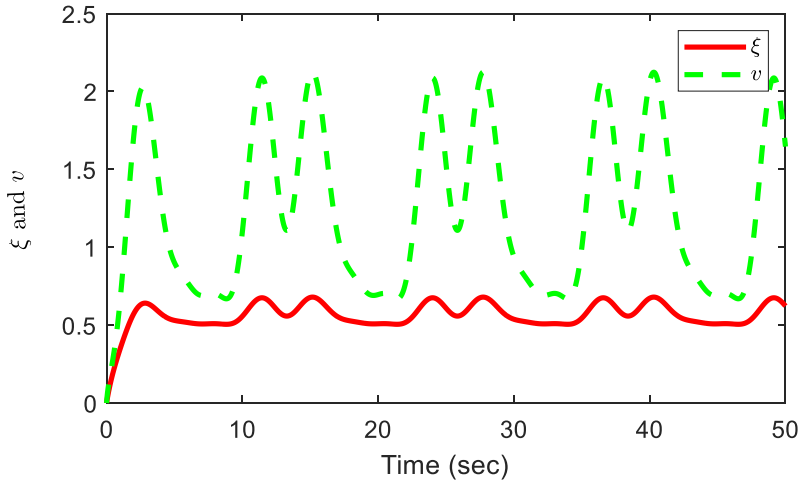

Figure 15. Dynamic behavior of ξ and v.

For Example 2, the tracking error z_1 responses of both methods are depicted in Figure 16 to provide a clearer and more intuitive comparison. It can be seen that the predefined-time control scheme delivers superior performance compared with the fixed-time method [42], as the tracking error under the proposed controller remains smoother and exhibits noticeably smaller fluctuations. Figure 16 highlights the improved transient characteristics and tighter error bounds achieved by the proposed predefined-time controller in this example.

Comparison under different initial conditions: To demonstrate the robustness of the proposed predefined-time control scheme, simulations is conducted under three different sets of initial conditions. The tracking performance of both the proposed controller and the fixed-time controller [42] was evaluated using integral square error (ISE) and integral absolute error (IAE). The initial system states for the three cases are:

- **IC1:** $[x_1(0), x_2(0), x_3(0)]^T = [0.5,\ 0.5,\ 0.5]^T$
- **IC2:** $[x_1(0), x_2(0), x_3(0)]^T = [-0.6,\ 0.4,\ -0.3]^T$
- **IC3:** $[x_1(0), x_2(0), x_3(0)]^T = [0.3,\ -0.4,\ 0.6]^T$

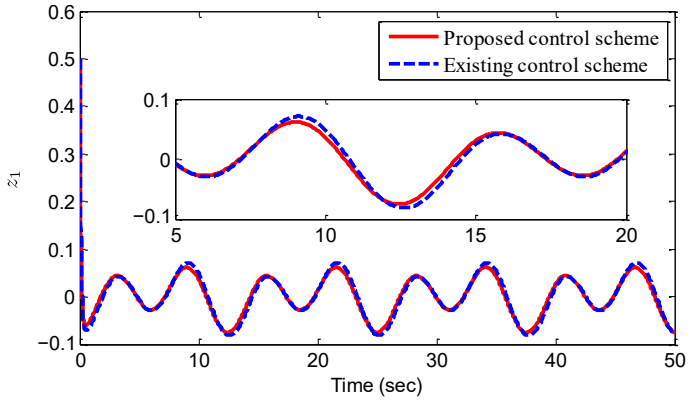

Figure 16. Trajectory of the tracking error z_1 under the proposed method and the existing method [42].

Table 5 presents a quantitative comparison of the two controllers under these initial system states.

Table 5. Comparison of performance indices between the proposed predefined-time controller and the fixed-time controller [42] under different initial conditions for Example 2.

Performance Index	IC1	IC2	IC3
Proposed ISE	26.4825	27.1043	26.2981
Fixed-time ISE [42]	28.7154	29.2879	28.6047
Proposed IAE	322.9997	328.4521	319.8745
Fixed-time IAE [42]	339.4872	344.2186	336.9053

The results indicate that the proposed predefined-time controller consistently achieves better tracking performance across all initial system states, with lower error accumulation and smoother trajectories than the fixed-time controller [42].

Comparison under different predefined times: To demonstrate the adjustability and effectiveness of the proposed predefined-time controller for Example 2, simulations were performed for three different values of the predefined convergence times, $T_{c_i} = 0.4$, 0.8, and 1.2 s. The performance was evaluated using the integral square error (ISE) and integral absolute error (IAE).

From Table 6, it can be observed that the tracking error remains within a small neighborhood of zero for all cases, and the proposed controller successfully achieves convergence within the specified T_{c_i}. While increasing T_{c_i} slightly affects the error metrics, the overall tracking performance remains accurate and stable. These results confirm that the proposed predefined-time control scheme allows the convergence time to be explicitly prescribed and effectively realized in practice for Example 2.

Table 6. Comparison of performance indices under different predefined times T_{c_i} for Example 2.

Performance Index	$T_{c_i} = 0.4$	$T_{c_i} = 0.8$	$T_{c_i} = 1.2$
ISE	26.4825	26.7153	26.9481
IAE	322.9997	325.2041	327.4102

Remark 8. *The proposed predefined-time adaptive control method provides a significant advancement over conventional finite-time and fixed-time control schemes. In finite-time control, the convergence of system states depends on the initial conditions, which makes the settling time unpredictable and limits the method's reliability in practical applications. Fixed-time control removes*

this dependence on initial conditions but still does not allow the designer to explicitly prescribe the convergence time, as it is implicitly determined by controller parameters. In contrast, the proposed predefined-time method allows the convergence time to be directly and explicitly specified in advance, ensuring predictable, precise, and reliable system behavior. This feature is particularly important for real-time and safety-critical applications, where timing accuracy and predictability are essential. Furthermore, the proposed method simultaneously addresses several practical challenges that are often neglected in conventional schemes. It is specifically designed for nonstrict-feedback nonlinear systems while compensating for unmodeled dynamics and input delays. By integrating a unified adaptive framework with command-filtered backstepping, the method also reduces computational complexity and mitigates approximation errors caused by command filters. Comparative studies with fixed-time control, as shown in Tables 1–4, demonstrate that the proposed predefined-time method not only ensures convergence within the prescribed time but also achieves slightly better performance indices and maintains consistent behavior under varying initial conditions. Overall, this approach combines predictable convergence, robustness to uncertainties, reduced computational burden, and enhanced performance, making it highly suitable for practical implementation in complex nonlinear systems and safety-critical applications.

5. Conclusions

This work proposes a predefined-time adaptive neural control strategy tailored for a class of nonlinear systems in nonstrict-feedback form, which are influenced by input delays and unknown dynamic uncertainties. To alleviate the computational burden typically associated with conventional backstepping techniques, a command-filtered backstepping approach integrated with error compensation is adopted. RBFNNs are employed to approximate the system's unknown nonlinear functions, while a dynamic auxiliary signal is incorporated to effectively manage the impact of unmodeled dynamics. The input delay is addressed through Padé approximation and the use of an intermediate variable. The developed control scheme guarantees uniform boundedness of all signals in the closed-loop system and drives the tracking error into an arbitrarily small vicinity of the origin within a specified, predefined time. Simulation results and comparative studies confirm the robustness and performance of the control method. The current study considers only constant input delays, and the Padé approximation is applied under this assumption. This represents a limitation, as in practical applications, input delays may be unknown or time-varying, and external random disturbances such as sensor noise may also be present, which could affect estimation accuracy and overall control performance. Future work will focus on extending the proposed control framework to handle unknown or time-varying input delays and random disturbances by incorporating suitable adaptive or robust compensation techniques, ensuring reliable performance under practical uncertainty. Furthermore, future work will investigate the applicability of the proposed method to fourth-order nonlinear systems and explore its real-time implementation in practical engineering systems, including robotic manipulators, high-speed rail systems, and industrial chemical processes, to further validate its effectiveness and generality.

Author Contributions: Conceptualization, M.K. and P.M.; Methodology, M.K. and P.M.; Software, M.K.; Validation, M.K. and P.M.; Formal analysis, M.K. and P.M.; Investigation, M.K. and P.M.; Resources, P.M.; Data curation, M.K. and P.M.; Writing—original draft, M.K.; Writing—review and editing, M.K. and P.M.; Supervision, P.M.; Project administration, P.M.; Funding acquisition, P.M. All authors have read and agreed to the published version of the manuscript.

Funding: The authors gratefully acknowledge the support of the library staff at Leuphana University of Lueneburg, Germany. This publication was funded by the Open Access Publication Fund of Leuphana University Lueneburg, Germany. This work was funded by the Deanship of Graduate Studies and Scientific Research at Jouf University under grant No. (DGSSR-2025-02-01021).

Data Availability Statement: The original contributions presented in this study are included in the article. Further inquiries can be directed to the corresponding author.

Conflicts of Interest: The authors declare no conflicts of interest.

References

1. Ma, H.; Ren, H.; Zhou, Q.; Lu, R.; Li, H. Approximation-based Nussbaum gain adaptive control of nonlinear systems with periodic disturbances. *IEEE Trans. Syst. Man Cybern. Syst.* **2021**, *52*, 2591–2600. [CrossRef]
2. Liu, M.; Zhang, W. Adaptive fuzzy tracking control for a class of time-varying output constrained nonlinear systems with non-affine nonlinear faults. *ISA Trans.* **2024**, *149*, 115–123. [CrossRef] [PubMed]
3. Zhao, K.; Song, Y.; Chen, C.P.; Chen, L. Adaptive asymptotic tracking with global performance for nonlinear systems with unknown control directions. *IEEE Trans. Autom. Control* **2021**, *67*, 1566–1573. [CrossRef]
4. Zhao, D.; Ouyang, X.Y.; Zhao, N.N.; Zhang, F. Event-triggered low-computation adaptive output-feedback fuzzy tracking control of uncertain nonlinear systems. *ISA Trans.* **2024**, *144*, 86–95. [CrossRef]
5. Segheri, M.; Boudjemaa, F.; Nemra, A.; Bibi, Y. Model-free adaptive backstepping control for a class of uncertain nonlinear systems. *Trans. Inst. Meas. Control* **2024**, *46*, 1317–1330. [CrossRef]
6. Wei, Y.; Yu, X.; Feng, Y.; Chen, Q.; Ou, L.; Zhou, L. Event-triggered adaptive optimal tracking control for nonlinear stochastic systems with dynamic state constraints. *ISA Trans.* **2023**, *139*, 60–70. [CrossRef]
7. Ni, J.; Liu, L.; He, W.; Liu, C. Adaptive dynamic surface neural network control for nonstrict-feedback uncertain nonlinear systems with constraints. *Nonlinear Dyn.* **2018**, *94*, 165–184. [CrossRef]
8. Kharrat, M.; Krichen, M.; Alhazmi, H.; Mercorelli, P. Neural network-based adaptive fault-tolerant control for strict-feedback nonlinear systems with input dead zone and saturation. *J. Franklin Inst.* **2025**, *362*, 107471. [CrossRef]
9. Xie, H.; Jing, Y.; Dimirovski, G.M.; Chen, J. Adaptive fuzzy prescribed time tracking control for nonlinear systems with input saturation. *ISA Trans.* **2023**, *143*, 370–384. [CrossRef] [PubMed]
10. Kharrat, M. Neural networks-based adaptive fault-tolerant control for stochastic nonlinear systems with unknown backlash-like hysteresis and actuator faults. *J. Appl. Math. Comput.* **2024**, *70*, 1995–2018. [CrossRef]
11. Xu, H.; Yu, D.; Sui, S.; Chen, C.P. An event-triggered predefined time decentralized output feedback fuzzy adaptive control method for interconnected systems. *IEEE Trans. Fuzzy Syst.* **2022**, *31*, 631–644. [CrossRef]
12. Li, Y.; Fan, Y.; Li, K.; Liu, W.; Tong, S. Adaptive optimized backstepping control-based RL algorithm for stochastic nonlinear systems with state constraints and its application. *IEEE Trans. Cybern.* **2021**, *52*, 10542–10555. [CrossRef] [PubMed]
13. Cai, J.; Wang, W.; Guo, D.; Yang, Q.; Yan, Q. Adaptive backstepping control for a class of nonlinear systems with output modeling error and external disturbance. *Trans. Inst. Meas. Control* **2025**, 01423312251318793. [CrossRef]
14. Xin, C.; Li, Y.X.; Ahn, C.K. Adaptive neural asymptotic tracking of uncertain non-strict feedback systems with full-state constraints via command filtered technique. *IEEE Trans. Neural Netw. Learn. Syst.* **2022**, *34*, 8102–8107. [CrossRef]
15. Li, Y.; Tong, S. Command-filtered-based fuzzy adaptive control design for MIMO-switched nonstrict-feedback nonlinear systems. *IEEE Trans. Fuzzy Syst.* **2016**, *25*, 668–681. [CrossRef]
16. Yu, J.; Chen, B.; Yu, H.; Lin, C.; Zhao, L. Neural networks-based command filtering control of nonlinear systems with uncertain disturbance. *Inf. Sci.* **2018**, *426*, 50–60. [CrossRef]
17. Yu, J.; Shi, P.; Dong, W.; Lin, C. Command filtering-based fuzzy control for nonlinear systems with saturation input. *IEEE Trans. Cybern.* **2016**, *47*, 2472–2479. [CrossRef] [PubMed]
18. Chen, Z.; Niu, B.; Zhang, L.; Zhao, J.; Ahmad, A.M.; Alassafi, M.O. Command filtering-based adaptive neural network control for uncertain switched nonlinear systems using event-triggered communication. *Int. J. Robust Nonlinear Control* **2022**, *32*, 6507–6522. [CrossRef]
19. Wang, H.; Kang, S.; Zhao, X.; Xu, N.; Li, T. Command filter-based adaptive neural control design for nonstrict-feedback nonlinear systems with multiple actuator constraints. *IEEE Trans. Cybern.* **2021**, *52*, 12561–12570. [CrossRef]
20. Li, Y.X. Command filter adaptive asymptotic tracking of uncertain nonlinear systems with time-varying parameters and disturbances. *IEEE Trans. Autom. Control* **2021**, *67*, 2973–2980. [CrossRef]
21. Sun, W.; Su, S.F.; Xia, J.; Zhuang, G. Command filter-based adaptive prescribed performance tracking control for stochastic uncertain nonlinear systems. *IEEE Trans. Syst. Man Cybern. Syst.* **2020**, *51*, 6555–6563. [CrossRef]
22. Wang, S.; Xia, J.; Wang, X.; Yang, W.; Wang, L. Adaptive neural networks control for MIMO nonlinear systems with unmeasured states and unmodeled dynamics. *Appl. Math. Comput.* **2021**, *408*, 126369. [CrossRef]
23. Chen, C.Y.; Tang, Y.; Lu, M.; Yan, H.; Huang, T. Robust adaptive neural control for a class of perturbed nonlinear systems with unmodeled dynamics and output disturbances. *Int. J. Robust Nonlinear Control* **2022**, *32*, 8189–8210. [CrossRef]
24. Shi, X.; Xu, S.; Jia, X.; Chu, Y.; Zhang, Z. Adaptive neural control of state-constrained MIMO nonlinear systems with unmodeled dynamics. *Nonlinear Dyn.* **2022**, *108*, 4005–4020. [CrossRef]

25. Chen, Y.; Liu, Y.J.; Liu, L.; Tong, S.; Xu, T. Event-triggered adaptive stabilization control of stochastic nonlinear systems with unmodeled dynamics. *Int. J. Robust Nonlinear Control* **2023**, *33*, 5322–5336. [CrossRef]
26. Wang, H.; Ma, J.; Zhang, H. Adaptive neural tracking control for high-order nonlinear systems with unmodeled dynamics and sensor fault. *IEEE Trans. Circuits Syst. II Express Briefs* **2023**, *71*, 1201–1205. [CrossRef]
27. Wang, H.; Liu, P.X.; Xie, X.; Liu, X.; Hayat, T.; Alsaadi, F.E. Adaptive fuzzy asymptotical tracking control of nonlinear systems with unmodeled dynamics and quantized actuator. *Inf. Sci.* **2021**, *575*, 779–792. [CrossRef]
28. Kharrat, M. Adaptive fault-tolerant control for a class of nonstrict-feedback nonlinear systems with unmodeled dynamics and dead-zone output using multi-dimensional Taylor networks. *Nonlinear Dyn.* **2024**, *112*, 13289–13306. [CrossRef]
29. Shen, F.; Wang, X.; Yin, X. Adaptive control based on barrier Lyapunov function for a class of full-state constrained stochastic nonlinear systems with dead-zone and unmodeled dynamics. *Trans. Inst. Meas. Control* **2021**, *43*, 1936–1948. [CrossRef]
30. Kharrat, M. Neural network-based adaptive finite-time command-filter control for nonlinear systems with input delay and input saturation. *Int. J. Adapt. Control Signal Process.* **2025**, *39*, 231–243. [CrossRef]
31. Xia, X.; Zhang, T.; Kang, G.; Fang, Y. Adaptive control of uncertain nonlinear systems with discontinuous input and time-varying input delay. *IEEE Trans. Syst. Man Cybern. Syst.* **2022**, *52*, 7248–7258. [CrossRef]
32. Wang, H.; Liu, S.; Yang, X. Adaptive neural control for nonstrict-feedback nonlinear systems with input delay. *Inf. Sci.* **2020**, *514*, 605–616. [CrossRef]
33. Wu, X.; Ding, S.; Xu, N.; Niu, B.; Zhao, X. Periodic event-triggered bipartite containment control for nonlinear multi-agent systems with input delay. *Int. J. Syst. Sci.* **2024**, *55*, 2008–2022. [CrossRef]
34. Li, D.P.; Liu, Y.J.; Tong, S.; Chen, C.P.; Li, D.J. Neural networks-based adaptive control for nonlinear state constrained systems with input delay. *IEEE Trans. Cybern.* **2018**, *49*, 1249–1258. [CrossRef]
35. Liu, S.; Zhao, N.; Zhang, L.; Xu, N. Adaptive neural hierarchical sliding mode control for uncertain switched underactuated nonlinear systems against unmodeled dynamics and input delay. *Asian J. Control* **2025**, *27*, 1552–1569. [CrossRef]
36. Cao, B.; Nie, X.; Wu, Z.; Xue, C.; Cao, J. Adaptive neural network control for nonstrict-feedback uncertain nonlinear systems with input delay and asymmetric time-varying state constraints. *J. Franklin Inst.* **2021**, *358*, 7073–7095. [CrossRef]
37. Cai, J.; Guo, D.; Wang, W. Adaptive fault-tolerant control of uncertain systems with unknown actuator failures and input delay. *Meas. Control* **2024**, *58*, 923–934. [CrossRef]
38. Zheng, X.Y. Adaptive neural control for nonstrict-feedback stochastic nonlinear systems with input delay. *Trans. Inst. Meas. Control* **2024**, *46*, 104–115. [CrossRef]
39. Kharrat, M.; Krichen, M.; Alhazmi, H.; Mercorelli, P. Neural network-based finite-time control for stochastic nonlinear systems with input dead-zone and saturation. *Arab. J. Sci. Eng.* **2025**, *50*, 1–11. [CrossRef]
40. Mei, Y.; Wang, J.; Park, J.H.; Shi, K.; Shen, H. Adaptive fixed-time control for nonlinear systems against time-varying actuator faults. *Nonlinear Dyn.* **2022**, *107*, 3629–3640. [CrossRef]
41. Kharrat, M.; Alhazmi, H. Adaptive finite-time neural control of nonstrict-feedback nonlinear systems with input dead-zone and output hysteresis. *Int. J. Gen. Syst.* **2025**, *54*, 71–94. [CrossRef]
42. Chen, M.; Li, Y.; Wang, H.; Peng, K.; Wu, L. Adaptive fixed-time tracking control for nonlinear systems based on finite-time command-filtered backstepping. *IEEE Trans. Fuzzy Syst.* **2022**, *31*, 1604–1613. [CrossRef]
43. Wu, Z.; Zhang, J.; Xing, L.; Sun, L. Fixed-time command-filtered control for nonlinear systems with mismatched disturbances. *Mathematics* **2024**, *12*, 3816. [CrossRef]
44. Ma, J.; Wang, H.; Qiao, J. Adaptive neural fixed-time tracking control for high-order nonlinear systems. *IEEE Trans. Neural Netw. Learn. Syst.* **2022**, *35*, 708–717. [CrossRef]
45. Liang, Y.; Li, Y.X.; Hou, Z. Adaptive fixed-time tracking control for stochastic pure-feedback nonlinear systems. *Int. J. Adapt. Control Signal Process.* **2021**, *35*, 1712–1731. [CrossRef]
46. Yang, Y.; Sui, S.; Chen, C.P. Adaptive predefined-time control for stochastic switched nonlinear systems with full-state error constraints and input quantization. *IEEE Trans. Cybern.* **2025**, *55*, 2261–2272. [CrossRef]
47. Wang, L.; Niu, J.; Wang, W. Predefined-time fuzzy output feedback control for nonlinear systems with multiple actuator constraints. *Int. J. Fuzzy Syst.* **2024**, *26*, 1–11. [CrossRef]
48. Cui, M.; Tong, S. Predefined-time fuzzy adaptive output feedback control for nonstrict-feedback stochastic nonlinear systems with state constraints. *Neural Comput. Appl.* **2024**, *36*, 3037–3048. [CrossRef]
49. Li, H.; Yang, F.; Liu, Z. Command filter-based adaptive predefined-time control for nonstrict-feedback nonlinear systems with unmodeled dynamics. *J. Franklin Inst.* **2024**, *361*, 106936. [CrossRef]
50. Gong, Y.; Guo, Y.; Li, D.; Ma, G.; Ran, G. Predefined-time tracking control for high-order nonlinear systems with control saturation. *Int. J. Robust Nonlinear Control* **2022**, *32*, 6218–6235. [CrossRef]
51. Jiang, Z.P.; Praly, L. Design of robust adaptive controllers for nonlinear systems with dynamic uncertainties. *Automatica* **1998**, *34*, 825–840. [CrossRef]

52. Zhang, J.; Yu, Z.; Zhu, Q.; Yu, X. Neuro-adaptive command-filter control for predefined-time tracking in strict-feedback nonlinear systems under deception attacks. *Mathematics* **2025**, *13*, 742. [CrossRef]
53. Chen, P.; Tan, J.; Yao, Y.; Zhang, X.; Yao, Y. Predefined-time adaptive fuzzy control for nonlinear systems with input saturation and deferred restriction. *Nonlinear Dyn.* **2025**, *113*, 4727–4744. [CrossRef]
54. Wang, L.; Han, Z.; Wang, W. Predefined-time fuzzy adaptive decentralized control for interconnected systems against multiple input signal constraints. *Nonlinear Dyn.* **2025**, *114*, 1–13. [CrossRef]
55. Su, L.; Jin, L.; Wang, J.; Shen, H. Adaptive predefined-time quantized tracking control for switched nonlinear systems using command-filter backstepping. *Int. J. Robust Nonlinear Control* **2024**, *34*, 9040–9054. [CrossRef]
56. Pan, Y.; Chen, Y.; Liang, H. Event-triggered predefined-time control for full-state constrained nonlinear systems: A command filtering error compensation method. *Sci. China Technol. Sci.* **2024**, *67*, 2867–2880. [CrossRef]
57. Kharrat, M.; Alhazmi, H. Fixed-time adaptive control for nonstrict-feedback nonlinear systems with input delay and unknown backlash-like hysteresis. *Neural Process. Lett.* **2025**, *57*, 52. [CrossRef]